

AD-A015 831

GROWTH OF MULTICOMPONENT COMPOSITES FROM THE MELT

Kenneth P. Young, et al

Massachusetts Institute of Technology

Prepared for:

Air Force Materials Laboratory

August 1975

DISTRIBUTED BY:

**NTIS**

National Technical Information Service  
U. S. DEPARTMENT OF COMMERCE

AFML-TR-75-16

296064

ADA 015831

# GROWTH OF MULTICOMPONENT COMPOSITES FROM THE MELT

MASSACHUSETTS INSTITUTE OF TECHNOLOGY  
CAMBRIDGE, MASSACHUSETTS 02139

AUGUST 1975

TECHNICAL REPORT AFML-TR-75-16  
FINAL REPORT FOR PERIOD MARCH 1971 to JULY 1974

DDC  
RECEIVED  
OCT 10 1975  
C

Approved for public release; distribution unlimited

Prepared for  
AIR FORCE MATERIALS LABORATORY  
AIR FORCE WRIGHT AERONAUTICAL LABORATORIES  
Air Force Systems Command  
Wright-Patterson Air Force Base, Ohio

Reproduced by  
NATIONAL TECHNICAL  
INFORMATION SERVICE  
US Department of Commerce  
Springfield, VA. 22151





**UNCLASSIFIED**

SECURITY CLASSIFICATION OF THIS PAGE(When Data Entered)

Further experimental work has been conducted on the effects of shape and direction variations on both the binary Al-Cu and ternary Al-Cu-Ni eutectic in-situ composites. These are discussed with respect to their influence on the rod on lamellae alignment and consequently the mechanical properties of the composite.

Additionally, a theory is given which relates the composition of interdendritic "eutectic" forming during unidirectional solidification to solidification variables. This theory shows that the composition of the solid freezing from the interdendritic liquid is not equal to the eutectic composition but is exactly equivalent to the composition of the alloy which would just grow with a planar front at the same growth rate and temperature gradient. It is shown that this leads to a method for determining the critical values of temperature gradient and growth rate for interface stability of off-eutectic composites. Experimental results for the binary Al-Cu system and the ternary Al-Cu-Ni system give good agreement with theory.

**UNCLASSIFIED**

SECURITY CLASSIFICATION OF THIS PAGE(When Data Entered)

## FOREWORD

This final report was prepared by K. P. Young, E. M. Dunn, L. Buchakjian, R. M. Sharp and M. C. Flemings. It covers work sponsored by the Air Force Materials Laboratory (AFML), Wright-Patterson Air Force Base, Ohio, from 1 March 1973 to the termination date, 1 July 1974 under contract F33615-71-C-1374 Task No. 735306. Previous reports under this contract have been issued in March 1972 (AFML-TR-72-161) and August 1973 (AFML-TR-73-208).

The work was performed in the Department of Materials Science and Engineering, Massachusetts Institute of Technology, under the direction of Capt. D. A. Rice and Capt. R. R. Smyth, Project Engineers.

The principal investigator is Professor M. C. Flemings, assisted by Dr. K. P. Young.

## TABLE OF CONTENTS

<u>SECTION</u>	<u>PAGE</u>
FOREWORD	
LIST OF FIGURES	
I. INTRODUCTION	1
Off Eutectic, In-Situ Composites (Solidified with Plane Front)	1
Eutectic In-Situ Composites; Effect of Change in Growth Direction and Cross-Section	4
Summary of Air Force Sponsored Work at M.I.T.	6
PART I. GROWTH OF TWO PHASE COMPOSITES FROM A TERNARY MELT	10
Apparatus and Experimental Procedure	10
Results	13
Microstructures	13
Stability Criterion	14
CONCLUSIONS TO PART I	17
PART II. EUTECTIC IN-SITU COMPOSITES: EFFECT OF CHANGE IN GROWTH DIRECTION AND CROSS-SECTION	18
Experimental Procedure	18
Experimental Results and Discussion	18
(1) Gradual Changes in Specimen Cross-Section	19
(2) Abrupt Contraction of Cross Section with Simultaneous Change of Growth Direction	21
(3) Abrupt Changes in Growth Direction with Constant Cross-Section	22
CONCLUSIONS TO PART II	24

<u>SECTION</u>	<u>PAGE</u>
PART III. THE COMPOSITION OF INTERDENDRITIC EUTECTIC	26
Binary Alloys	26
Ternary Alloys	29
Experimental Apparatus and Procedure	32
Results and Discussion	33
CONCLUSIONS TO PART III	36
APPENDIX A	37
APPENDIX B	39
REFERENCES	48

## LIST OF FIGURES

<u>Figure</u>	<u>Page</u>
I. Various possible microstructures obtained from three-phase alloys, in order of increasing G/R.	9
1. Composition ranges of specimens used by Rinaldi et al and the present work. (Ternary section from ref. 14.)	50
2. Schematic representation of the furnace-chill assembly of the apparatus used by Rinaldi et al.	51
3. High gradient crystal growth apparatus. (1) Lava plug, (2) Fiberfrax insulation, (3) Viton O-ring, (4) coolant water in, (5) alumina crucible 1/4 in. diameter, (6) furnace thermocouple, (7) stainless steel housing, (8) platinum-rhodium heating strip, inside wound, .010"x.0625", (9) brass chill chamber, (10) coolant water out, (11) specimen thermocouple, (12) element electrical connection.	52
4. Ingot #20, 6.0 wt% Ni, 1.01 wt% Cu, $G/R = 4.1 \times 10^5$ °Csec/cm <sup>2</sup> , single-phase cells, two-phase cells, and three-phase composite structure. (a) Transverse section, 100X. (b) Longitudinal section, 100X.	53
5. Ingot #26, 8.85 wt% Ni, 0.92 wt% Cu, $G/R = 10.5 \times 10^5$ °Csec/cm <sup>2</sup> , single-phase cells and two-phase composite. (a) Transverse section, 100X. (b) Longitudinal section, 100X.	54
6. Ingot #11, 5.15 wt% Ni, 0.95 wt% Cu, $G/R = 4.85 \times 10^5$ °Csec/cm <sup>2</sup> , two-phase composite structure. (a) Transverse section, 100X. (b) Longitudinal section, 100X.	55
7. (a) 1.5 wt% Cu + 5.85 wt% Ni, $G/R = 2.73 \times 10^5$ °Csec/cm <sup>2</sup> , two-phase cells and three-phase composite structure. Transverse section, 200X (after Rinaldi, Sharp and Flemings <sup>3</sup> ). (b) Ingot #21, 6.6 wt% Ni + 1.01 wt% Cu, $G/R = 1.94 \times 10^5$ °Csec/cm <sup>2</sup> , single-phase cells, two-phase cells, and three-phase composite structure. Longitudinal section taken near the quenched liquid-solid interface, 500X.	56
8. Aluminum-rich corner of Al-Cu-Ni system.	57

<u>Figure</u>	<u>Page</u>
9. Structure of directionally solidified ingots as a function of G/R and $C_{ONi}$ with $C_{OCu} = 1 \text{ wt\%Cu}$ . *Reference Rinaldi, Sharp and Flemings.	58
10. Al-Cu-Ni Liquidus Surface.	59
11. Cu distribution ahead of the quenched composite interface of ingot #1.	60
12. Ni distribution ahead of the quenched composite interface of ingot #1.	61
13. $\ln(C_L - C_S)$ for Cu versus distance from the quenched interfaces in ingot #'s 1, 11 and 19.	62
14. $\ln(C_L - C_S)$ for Ni versus distance from the quenched interface in ingot #1.	63
15. Al-Cu-Ni ternary system, 600°C isotherm (after Koster, Zwicker and Moeller <sup>14</sup> ).	64
16. Cross-sectional view of crucible and insert system.	65
17. Insert b, lower portion, structure aligned in the original growth direction, longitudinal view, 115X. (a) Sample No. 0008, binary Al-Ni eutectic, $\theta = 18^\circ$ . (b) Sample No. 0014, ternary Al-Ni-Cu eutectic, $\theta = 10^\circ$ , corresponding schematic Figure 18.	66
18. Schematic view of insert type b, $\theta > 8^\circ$ , showing the structure orientated in the original growth direction.	67
19. Sample No. 0017, insert type b, ternary Al-Ni-Cu eutectic, upper portion, structure follows the contour of the insert, $\theta = 6^\circ$ , longitudinal view, 115X. Corresponding schematic Figure 20.	68
20. Schematic view of insert type b, $\theta < 8^\circ$ , showing the structure following the contour of the insert at the upper portion.	69
21. Lamellae spacing as a function of growth rate for ternary Al-Ni-Cu eutectic, Rinaldi's data <sup>3</sup> for compositions containing from 17.5 to 12.3 at. pct. Cu and from 0.0 to 1.32 at. pct. Ni, Chadwick's <sup>22</sup> data for the Al-Cu binary eutectic.	70
22. Sample No. 0014, ternary Al-Ni-Cu eutectic, transverse view, 1150X.	71

<u>Figure</u>	<u>Page</u>
23. Solidification rate at various percentages of initial cross-sectional area into the portions of insert type b, ternary Al-Ni-Cu eutectic.	72
24. Sample No. 0020, insert type a, ternary Al-Ni-Cu eutectic, lower portion, viewed under polarized light, $\theta = 20^\circ$ , longitudinal view, 115X.	73
25. (a) Sample No. 0003, insert type a, binary Al-Ni eutectic, lower portion, location of liquid-solid interface, $\theta = 14^\circ$ , longitudinal view, 115X. (b) Schematic.	74
26. Insert type a, middle portion after the bend, downward face, depleted zone, longitudinal view, 115X. (a) Sample No. 0004, binary Al-Ni, $\theta = 14^\circ$ . (b) Sample No. 0013, ternary Al-Ni-Cu, $\theta = 14^\circ$ , corresponding schematic Figure 27.	75
27. Schematic view of insert type a, $\theta > 8^\circ$ , showing the different grain orientations developed.	76
28. Schematic illustration of the unidirectional solidification of cells of a binary alloy: (a) phase diagram, (b) showing the concentration of solute as a function of distance.	77
29. Schematic illustration showing the growth of cells or dendrites in a ternary system. (a) Phase diagram showing solidification path (full line) and diffusion path for a planar interface (dashed line). (b) Inter-cellular liquid composition. Primary phase solidifies first and, when the liquid composition reaches $C_{2t}$ , two-phase material is formed.	78
30. Average concentration of interdendritic eutectic plotted as a function of G/R for the binary Al-CuAl <sub>2</sub> system. Also included are the theoretical lines calculated from equation 8 and the experimental results of Jordan and Hunt. <sup>24</sup>	79
31. Average copper concentrations of interdendritic eutectic plotted as in Figure 3 for ternary Al-Cu-Ni system. The theoretical line is calculated from equation 12.	80

## INTRODUCTION

### Off Eutectic, In-Situ Composites (Solidified with Plane Front)

The growth of aligned in-situ composites from the melt offers inherent advantages for high temperature applications over other methods of manufacture since problems of achieving low reactivity and sufficient bonding between the phases are avoided. Excellent high temperature properties have now been obtained in several alloy families. Bibring et al<sup>1</sup> have recently demonstrated that the high temperature properties of aligned Co-TaC alloys are more than twice that of the non-aligned structure.

The early work on aligned composite growth employed alloys of eutectic or near eutectic compositions. However, in 1967, Mollard and Flemings<sup>2</sup> showed that with sufficiently large values of G/R (thermal gradient divided by growth rate) equivalent structures could be obtained in binary alloys well removed from the eutectic composition. They successfully applied a simple constitutional supercooling model and found the necessary conditions for plane front growth to be:

$$G/R \geq -m \frac{(C_E - C_0)}{D} \quad (1)$$

where m is the liquidus slope, D the solute diffusivity in the liquid and C<sub>E</sub> the eutectic composition, which for binary alloys is the composition of the liquid at the liquid/solid interface.

However, aligned composites for actual use in high temperature applications will almost certainly be multi-component alloys, and the major ultimate practical significance of the Mollard-Flemings

study is that the several principles can be generalized to these multi-component systems. The principles are:

1. Provided interface kinetics do not pose too great a barrier to growth, any multicomponent alloy can be grown with plane front (and hence with aligned composite microstructure) provided G/R is sufficiently high and convection sufficiently low.
2. The number of phases present in the final structure is the number that would be present after equilibrium solidification.

Thus, for example, in a ternary system, a two phase aligned composite can be grown with the third element in solid solution in one or both phases. In a different region of the ternary phase diagram a three phase aligned composite can be grown. The general principles outlined above make it possible to "tailor" both the alloy and microstructure. Thus, solid solution elements can be added for improving corrosive resistance or hot strength, and volume fractions of the phases present can also be varied as desired. This is, of course, subject to the engineering limitations in achieving high G/R values.

Rinaldi, Sharp and Flemings<sup>3</sup> extended the constitutional supercooling analysis to the ternary aluminum-copper-nickel system. Again, they arrived at a criterion for plane front growth in a ternary alloy of composition  $C_{om}$ ,  $C_{on}$ :

$$G/R > -p \frac{(C_{Lm}^* - C_{om})}{D_{mm}} - s \frac{(C_{Ln}^* - C_{on})}{D_{nn}} \quad (2)$$

where p and s are the liquidus slopes given by :  $p = \frac{\partial T}{\partial C_{Lm}}$

$s = \frac{\partial T}{\partial C_{Ln}}$  and  $C_{Lm}^*$  and  $C_{Ln}^*$  are the liquid concentrations at the solid/liquid interface of elements m and n respectively.

For a three phase composite, the liquid in front of the interface is of ternary eutectic composition  $C_E$  and so the stability criterion can be rewritten:

$$G/R > -p \frac{(C_{Em} - C_{Om})}{D_{mm}} - s \frac{(C_{En} - C_{On})}{D_{nn}} \quad (3)$$

Rinaldi et al verified their analysis with the three groups of alloys shown in Figure 1. Two of these lie about the ternary eutectic compositions and yielded 3 phase composites while the third represented essentially the binary Al-Ni eutectic with minor additions of copper. They found reasonably good agreement with their theoretical predictions of interface breakdown.

The first part of the work contained herein is a continuation of the experimental work of Rinaldi et al. Alloys of approximately constant wt%Cu and varying Ni content were used within the range shown in Figure 1. These alloys solidify with plane front to yield a two phase composite. They represent a potentially useful type of alloy since the third component, Cu in this case, solution strengthens one of the composite phases and may subsequently be used to provide precipitation hardening.

Many of the alloys which are likely candidates for use as high temperature composites contain a phase which is strongly faceting. An example is the TaC phase in a cobalt-chromium matrix. Little is known quantitatively about the stability requirements for alloys such as these when the faceting phase is present in relatively large

quantities. For this reason, particular attention was paid in this work to alloys from a portion of the Al-Cu-Ni ternary system in which faceted  $\text{NiAl}_3$  plus  $\alpha\text{Al}$  is observed. (Figure 1)

#### Eutectic In-Situ Composites; Effect of Change in Growth Direction and Cross-Section

The second part of the present work is an experimental investigation of the behavior of aligned composite structures when confronted with angular or cross sectional changes during growth. This is an area which has significant engineering importance but in which published data is scarce. Notable among those, Hunt et al<sup>4,5</sup> have examined the behavior of binary tin, lead and cadmium base eutectics when confronted with a partial obstruction and Chadwick et al<sup>7,8</sup> have experimented with "J" shaped ingots of varying radii of curvature. Also analysis by Curran and Erickson<sup>9</sup> has shown that the parameter to cross sectional area ratio is of prime importance in the solidification of turbine blade configurations. More recently, Farag and Flemings<sup>10</sup> have studied the influence on the binary Al-AlNi eutectic of shape variations which were both gradual and abrupt and this present work has followed from that investigation.

Alloys of the binary (Al-Ni) and ternary (Al-Cu-Ni) eutectic composition have been used to avoid morphological complications arising from changes in G/R or solute accumulation induced by the geometrical variations.

Additionally, a theory is given which relates the composition of interdendritic "eutectic" forming during unidirectional solidification to solidification variables. This theory has been developed as the basis of previous work under this contract and correlates well with experimental measurements reported herein.

### Summary of Air Force Sponsored Work at M.I.T.

At this termination date of Air Force Sponsored research at M.I.T. on in-Situ composites, it is appropriate to summarize the results of that work. The work was contracted on 1 March, 1971, and completed on 1 July, 1974. In that time three reports (including this one) were issued. A total of five papers published, and two additional papers are being prepared for publication.

The first report<sup>i</sup> and associated papers<sup>iv,v</sup> describe the work on ternary alloys of Rinaldi et al that extends the principles of growth of in-Situ composites to ternary alloys. This work has also been summarized in several review papers<sup>xi-xiii</sup> and in a recently published text.<sup>xiv</sup>

The second report<sup>ii</sup>, and a related paper<sup>vi</sup> extend the ideas of directionally solidified in-situ composites to growth of non-planar, cellular type structures. Such structures have the advantage of more directionality than the usual columnar dendritic directionally solidified structures. At the same time, they can be grown at substantially lower G/R (e.g. higher rates) than eutectic-like in-situ composites.

This work is of potential great engineering importance. The structures so produced should have a useful combination of desirable processing characteristics and final properties. Such structures have not as yet been exploited. Figure I (P. 9) from this study shows examples of these types of structures for a ternary three phase alloy. Structures (c) and (d) of that Figure, are two "cellular-composite: structures of the type that has not been exploited commercially. They are compared in the Figure with structures now

being explored or studied in detail. Structures (a) and (b) are the conventional equiaxed and columnar dendritic type, obtained at very low G/R. Structure (e) is the in-situ composite obtained at very high G/R.

Several additional papers of fundamental importance have arisen from the foregoing work on "cellular-composites"<sup>vi,viii</sup>. In one, it is shown that the "eutectic" within dendritic or cellular structures is not of eutectic composition, but has a composition that depends on G/R. In another, a comparison is given of experimental data of another investigation, with theory of cellular solidification developed in work at M.I.T.

Publications emanating from Air Force Sponsored Research at M.I.T.

- i M.D. Rinaldi R.M. Sharp, M.C. Flemings, Tech. Report AFML-TR-72-161
- ii R.M. Sharp, M.C. Flemings Tech Report, AFML-TR-73-208.
- iii K. P. Young, E. M. Dunn, L. Buchakjian, R. M. Sharp, M. C. Flemings, This Report, AFML-TR-75-16.
- iv M.P. Rinaldi, R.M. Sharp, M.C. Flemings, Met. Trans. Vol 3, (1972) 3133-3138.
- v M.D. Rinaldi, R.M. Sharp, M.C. Flemings, *ibid* Vol 3, 3139-3148.
- vi R.M. Sharp, M.C. Flemings, Met. Trans, Vol. 4 (1973) 997-1001.
- vii R.M. Sharp, M.C. Flemings *ibid*, Vol 5 (1974) 823-830.
- viii R.M. Sharp, M.C. Flemings, *ibid*, Vol. 6A (1975) 936-937.
- ix E.M. Dunn, K.P. Young, M.C. Flemings, to be published.
- x L. Buchakjian, K.P. Young, to be published.
- xi M.C. Flemings, Howe Memorial Lecture, Met. Trans. Vol. 5 (1974) 2121.

- xii M.C. Flemings, *Scientific American*, Dec. 1974, 88-95.
- xiii R.M. Sharp, M.C. Flemings, Conf. on in-Situ composites, Lakeville, Connecticut, Sept. 1973.
- xiv M.C. Flemings, *Solidification Processing*, Chapter 4, McGraw Hill, (1974).

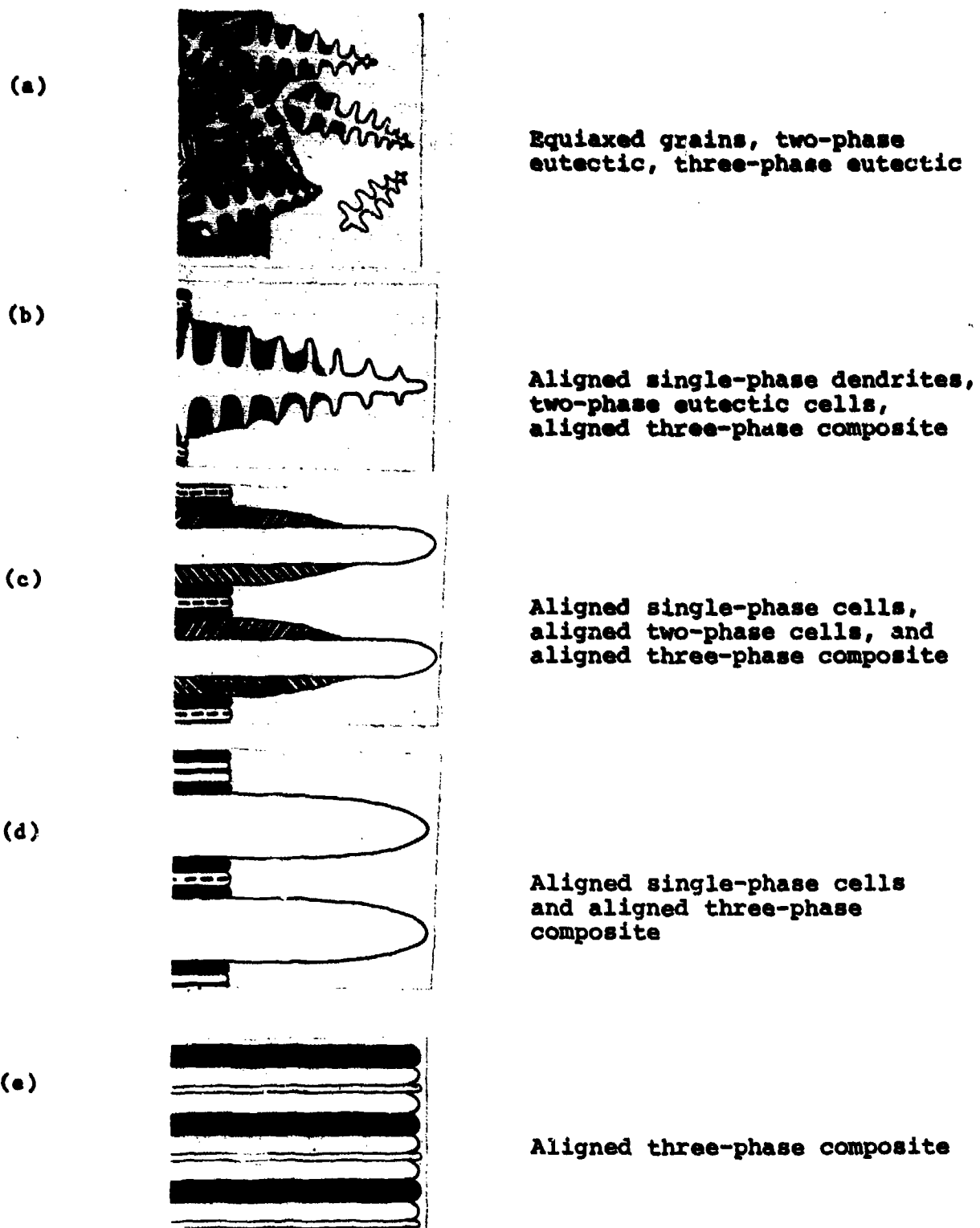


Figure I. Various possible microstructures obtained from three-phase alloys, in order of increasing G/R.

## PART I. GROWTH OF TWO PHASE COMPOSITES FROM A TERNARY MELT

### Apparatus and Experimental Procedure

The apparatus for directionally solidifying the aluminum-copper-nickel alloys at a high thermal gradient and controlled low growth rate was, for the initial work, essentially the same as that used by Rinaldi, Sharp and Flemings,<sup>3</sup> Figure 2.

In order to maintain high temperature gradients and eliminate convection, a small specimen cross-section was called for. Rods of 1/8-inch diameter by 5 inches long were used. For chemical inertness and high thermal conductivity, high purity graphite (99.95%) was used as the crucible material. Crucible dimensions were 1/8-inch inside diameter, 5/16-inch outside diameter and 6 inches long. A twin-bore alumina tube, .035-inch outside diameter by 3-inches long enclosed the .004-inch chromel-alumel thermocouple wires. The thermocouple junction was extended approximately 0.10cm beyond the alumina tube and was coated with refractory cement. In this fashion, it was possible to directly monitor the thermal gradient in each specimen grown.

Subsequently, as this work was extended to study the influence of faceted phases upon the conditions for planar front growth, a new furnace was constructed to achieve the higher thermal gradients likely to be required.

Figure 3 shows a schematic diagram of the new apparatus. The resistance wound furnace consists of platinum-20% rhodium strip (.010" x 1/16") wound in the interior of an alumina tube. This was accomplished by winding the strip between the glands of a threaded graphite rod (1/12" diameter) and coating with an alumina cement

(#1139 + 3 wt% polyvinyl-alcohol). The assembly was placed in a furnace at 1300°C in order to sinter the alumina and to decompose the graphite into CO<sub>2</sub> gas.

This design makes it possible to obtain higher furnace temperatures and therefore thermal gradients than in conventional externally wound tube furnaces. Also, since the platinum-20% rhodium strip has a high surface to volume ratio, and the surface is exposed to the interior of the furnace, the furnace windings can dissipate energy more efficiently. The temperature of the furnace is monitored with a platinum-10% rhodium thermocouple placed within .5 cm of the furnace windings.

The chill system in both designs is composed essentially of a cylindrical brass chill, a constant temperature reservoir, and a pump. The coolant water is pumped through a coil in the ice-water reservoir, through the brass chill, and finally through a sump before repeating the cycle. The sample passes through the brass cylinder which is sealed at the top and bottom with O-rings. The ice-water reservoir eliminates fluctuations in the coolant temperature, whereas the sump removes air from the cooling system.

Two master alloys (approximately 10 kg each) of aluminum-nickel and aluminum-copper were prepared from high purity aluminum (99.99%), copper (99.9%) and nickel (99.9%). Ternary alloys (approximately 2 kg each) were then prepared by mixing the two master alloys. The graphite crucible filling technique employed for the early part of this work represented a departure from that of Rinaldi, Sharp and Flemings<sup>11</sup>. A 200 gram alloy charge was prepared and induction melted under vacuum. Return to atmospheric pressure after insertion of the graphite tubes into the charge

caused filling. One-inch specimens were cut from the end of each filled tube and were subjected to wet chemical analysis. With the adoption of the new apparatus, recrystallized alumina crucibles, which are sensitive to thermal shock, were used and were filled in the manner described by Rinaldi et al.

To begin a run, the filled specimen was placed in the furnace as previously described. When the furnace reached constant temperature (as measured by the Pt-10% Rh thermocouple), the specimen was driven upwards into the furnace. The sample position was monitored by means of a fixed pointer attached to the drive system. When the specimen thermocouple was approximately 1 cm past the liquid-solid interface, the sample was held in position approximately 10 minutes to reach equilibrium. The direction of specimen motion was then reversed and 4 cm of the specimen were solidified at a controlled rate. The remaining portion of the specimen was rapidly quenched in the chill at the end of each experiment.

The thermocouple in each specimen provides the data necessary to determine the thermal gradient in the liquid at the liquid-solid interface. The growth rate was determined by monitoring the pointer system described earlier.

Each specimen was mounted and sectioned for metallographic study. A transverse section was taken at about 2 cm from the quenched liquid-solid interface. A longitudinal section containing the quenched interface was also mounted.

An electron beam microanalyzer was used to measure the solute distribution ahead of the quenched interface in several composite specimens. A 25 micron round spot was used. The background level was at an extremely low value, 5 counts per second.

## Results

The specimens examined in this study ranged in composition from 3.92 to 8.85% nickel. The copper content was kept at a constant value of approximately 1%. This places the specimens on the dark line shown in Figure 1. The specimens were in the two-phase region of the aluminum-copper-nickel ternary system. The microstructures consisted of the  $\alpha$  and  $\epsilon$  phases in various distributions and morphologies. The  $\alpha$  phase is a face-centered cubic solution of copper and nickel in aluminum. The  $\epsilon$  phase is  $\text{NiAl}_3$ , a faceted, orthorhombic structure. Table I is a list of specimens giving growth conditions used in the early study of two-phase composite growth and Table II lists those runs made to date in the high temperature gradient furnace in which thermal gradients of up to  $590^\circ\text{C cm}^{-1}$  have been achieved.

Several specimens were grown at each composition but at different values of G/R. By examining the microstructures obtained for the different values of G/R, it was possible to determine at which values plane front growth was possible.

## Microstructures

Since the range of compositions studied straddles the line of two fold saturation, low values of G/R, typically  $1 \times 10^5 \text{ }^\circ\text{C sec cm}^{-2}$ , resulted in interface breakdown in the form of either  $\alpha$  or  $\epsilon$  cells or dendrites. Figure 4 shows a typical structure obtained from a specimen containing 6.0 swt% Ni in which a faceted single phase  $\epsilon$  cell can be seen within a two-phase  $\alpha$  plus  $\epsilon$  cell boundary.

As G/R increased, two phase  $\alpha$  plus  $\epsilon$  cell boundaries were no

longer observed and structures were typically single-phase  $\alpha$  or  $\epsilon$  cells protruding ahead of and surrounded at their roots by two phase composites (Figure 5).

At still higher values of  $G/R$ , composite structures such as that shown in Figure 6 were obtained.

Finally of note are the micrographs of Figure 7. The upper transverse section has been taken from the report of Rinaldi et al<sup>11</sup> and as in Figure 4 shows no ternary eutectic phase between the cell boundaries. The lower longitudinal micrograph taken from the present work and from a specimen of similar composition grown under similar conditions shows that ternary eutectic is indeed present close to the quenched interface. With the aid of the Scheil equation:

$$f_e = (C_0/C_E)^{1/1-K}$$

an approximate volume fraction ternary eutectic ( $f_e$ ) may be calculated which for these alloys is less than 0.1%. Thus, solid state diffusion can easily diminish this quantity to zero in times comparable to the growth time. Since, Rinaldi et al took their transverse sections, some 1 cm behind the quenched interface, this would, at their typical growth rates, easily allow sufficient time for the complete disappearance of ternary eutectic phase.

#### Stability Criterion

A comparison between the observed transition points and those predicted by equation (2) was made. Diffusion coefficients can be sensitive to composition; therefore, rather than use the

data determined by Rinaldi et al<sup>11</sup> in other portions of the phase diagram, electron microprobe analysis ahead of the quenched interface of several specimens was used to determine  $D_{Cu}$  and  $D_{Ni}$  after the technique of Sharp<sup>12</sup>. This procedure was identical to that described by Rinaldi et al<sup>3</sup>, and yielded the following values:

$$D_{Cu} = 3.25 \times 10^{-5} \text{ cm}^2/\text{sec}$$

$$D_{Ni} = 1.74 \times 10^{-5} \text{ cm}^2/\text{sec}$$

$$\bar{K}_m = 0.189$$

The directional derivatives of the liquidus surface and  $C^*_{Ln}$  were obtained by an analysis of the phase diagram (Figure 8) outlined in Appendix B. The following results were obtained.

For  $C_{0n} < 5.5$  wt pct Ni

$$p = \frac{\partial T}{\partial C_{Lm}} = -3.16^\circ\text{C}/\text{wt pct Cu}$$

$$s = \frac{\partial T}{\partial C_{Ln}} = -3.5^\circ\text{C}/\text{wt pct Ni}$$

For  $C_{0n} > 5.5$  wt pct Ni

$$p = \frac{\partial T}{\partial C_{Lm}} = -1.58^\circ\text{C}/\text{wt pct Ni}$$

$$s = \frac{\partial T}{\partial C_{Ln}} = 18.6^\circ\text{C}/\text{wt pct Ni}$$

It was also determined that  $C^*_{Ln} = 5.32$  wt pct Ni.

Using these data a plot (Figure 9) was made indicating the composition, G/R and microstructure of each of the ingots listed in Tables I and II. For a given composition, the minimum value of G/R which would maintain plane-front growth was noted. The

curve marked "Experimental" connects these points. The curves labeled "Theoretical - Model I" and "Theoretical - Model II" were derived by insertion of different values of  $\bar{k}_M$ ,  $D_{Cu}$ ,  $D_{Ni}$ ,  $p$  and  $s$  taken from Appendices A and B into equation (2). Model I takes into account small variations in  $\bar{k}_M$  as determined from a model of the phase diagram. Model II assumes  $\bar{k}_M$  is approximately constant as measured experimentally by electron probe microanalysis. (i.e., nickel has a negligible effect on the solidus temperature). The resultant relationship in the case of Model II is:

for  $C_{0n} < 5.5$  wt pct Ni

$$G/R \geq 4.16 \times 10^5 + 2.01 \times 10^5 (5.3 - C_{0n}) \quad (4)$$

and for  $C_{0n} > 5.5$  wt pct Ni

$$G/R \geq 1.28 \times 10^5 - 10.6 \times 10^5 (5.3 - C_{0n}) \quad (5)$$

for the constant 1 wt pct Cu used in this study.

Figure 10 shows the liquidus surface for the Al-rich corner of the Al-Cu-Ni system. Data were obtained from references (13) and (14). A model of the liquidus surface developed in Appendix B, was used to approximate the liquidus near known isotherms.

## CONCLUSIONS TO PART I

1. The experimental data for growth of in-situ composites of Al rich Al Cu-Ni alloys in the two-phase region ternary system is in accord with a constitutional supercooling model for plane-front growth.
2. At quenched cellular liquid-solid interfaces intercellular ternary eutectic was observed. However, behind the interface, solid state diffusion reduces the amount of eutectic present.
3. Liquid diffusion coefficients were measured from the solute distributions ahead of the quenched liquid-solid interface. The values thus obtained were used in the calculation of the stability criterion.
4. A mathematical model of the liquidus surface was developed and used in the calculation of the stability criterion.

PART II. EUTECTIC IN-SITU COMPOSITES;  
EFFECT OF CHANGE IN GROWTH DIRECTION AND CROSS-SECTION

Experimental Procedure

Alloys of the approximate binary (Al-6.1 wt% Ni) and ternary (Al-0.73 wt% Ni - 32.94 wt% Cu) eutectic composition (see Figure 1 of Part I) were directionally solidified using the apparatus and technique described by Rinaldi et al.<sup>3,11</sup> Specimens were contained within a 4.8 mm inside diameter by 170 mm long graphite (99.95%) crucible. Growth was accomplished by withdrawing at the required rate from a platinum resistance furnace into a water-cooled copper chill and was terminated by rapid quenching. Variations in cross-section up to 90% and deviations in the growth direction of between 6 and 40°, characterized by the angle  $\theta$ , Figure 16, were obtained with the aid of graphite inserts. Temperature gradients within the specimen were controlled by the furnace temperature and were measured with a chromel/alumel thermocouple of 0.1 mm diameter wire insulated in twin bore 0.92 mm diameter alumina and located just below the bottom insert. A list of specimens and associated growth conditions is given in Table III.

Experimental Results and Discussion

In regions removed from the inserts, both the binary and the ternary eutectic alloys showed no change in morphologies with growth conditions except for variations in inter-rod, (in the case of the binary eutectic) or interlamellar spacings with growth rate. Thus, assuming solute effects to be negligible for eutectic compositions, the following observations within the inserts can be attributed to the shape and angular deviations they imposed upon the composites.

For simplicity, the results may be sub-divided into three groups:

1. Gradual changes in specimen cross-sectional area.
2. Abrupt contraction of cross-sectional area with simultaneous change of growth direction.
3. Abrupt changes in growth direction with constant cross-sections.

(1) Gradual Changes in Specimen Cross-Section

These observations relate to insert (b) of Figure 16 in which it can be seen exist regions of both converging and diverging cross-section, together with a short length of constant reduced cross-section. From experiments in which the specimens were quenched with the liquid-solid interface within the lower, converging, and middle, constant, cross-section regions of insert (b), it can be stated that within these regions the interface remained flat and perpendicular to the crucible axis.

In the mouth of the insert in which the cross-section is continuously converging, the lamellae and rods, consistent with previous work<sup>10</sup>, continued to grow parallel to the crucible axis regardless of the value of  $\theta$  and this persisted through the region of constant reduced cross-section also. Contrary to the results of Farag<sup>10</sup>, however, only a few specimens showed a slight tendency for the rods or lamellae to coarsen at the upper specimen/insert interface, although some depleted zones were apparent in most specimens (Figures 17 & 18). For the binary eutectic alloy, a transition of rod to plate morphology was observed for the  $Al_3Ni$  phase which was reversed as the cross-section diverged again. Such

observations have been reported previously<sup>10,17,18</sup> and attributed to various causes. The present results, discussed further below, support Hertzberg's<sup>18</sup> suggestion of a growth rate dependent transition. In all, it is considered that a converging solidification cross-section would not seriously impair the mechanical strength of these composites although for compositions removed from the eutectic, solute accumulation effects may prove harmful.

At the exiting end of the insert in which the specimen cross-section is continuously diverging, the structures depended on the value of  $\theta$ . For values of  $\theta$  greater than about  $8^\circ$ , all the rods or lamellae continued to grow parallel to the crucible axis such that their nucleation occurred on the upward facing insert wall. For values of  $\theta < 8^\circ$ , regions close to the insert wall exhibited rods or lamellae growing parallel to it (Figures 19 & 20) while the central region of the specimen continued to show no deviation in rod or lamellar direction from the crucible axis. Similar results were observed by Farag<sup>10</sup> although he reported a transition in growth structure at around  $20^\circ$  and also by Chadwick<sup>20</sup> who has shown essentially the same effect for diverging cross section with small or large radius of curvature. It would suggest that in such regions, the liquid/solid interface becomes curved; although it is unlikely that this would significantly weaken the structure since the rods and lamellae remain essentially aligned.

From an analysis of the rod or lamellar spacings,  $\lambda$ , in regions removed from the inserts, we have obtained for both alloys, the expected linear relation  $\lambda$  vs.  $R^{-\frac{1}{2}}$  shown in Figure 21 for the ternary eutectic alloy. Using a serial polishing technique, which yielded results typically shown in Figure 22, we have therefore been

able to translate lamellar or rod spacings within the insert into approximate growth rates. This yielded curves for both alloys as shown in Figure 23, which shows clearly how the growth rate drops with converging cross section and vice versa. The two scatter bands in this figure result from the grouping of various specimen withdrawal rates employed. Fluctuations within each band can be attributed to minor variations in the withdrawal rate and no correlation with  $\theta$  was obtained. The measured change in growth rate agrees well with Hertzberg's<sup>18</sup> explanation for the change from rod to plate morphology of the binary Al-Ni eutectic alloy.

(2) Abrupt Contraction of Cross Section with Simultaneous Change of Growth Direction

These observations related to the lower regions of insert (a) (Figure 16) and can be sub-divided with respect to the value of  $\theta$ . In regions to either side of the orifice of insert (a), regardless of  $\theta$ , the rods or lamellae, as reported previously<sup>10</sup>, simply grew into and terminated at the insert bottom face without deviation or morphology change. For  $\theta > 8^\circ$  in the region of the orifice, the matrix developed a multiple grain structure shown in Figure 24 with the aid of polarized light. The rods or lamellae of the grain near the upper insert wall grew parallel to the insert wall while those of the lowermost grain nucleated on the insert wall and continued to grow parallel to the crucible axis, and it was this grain which eventually dominated the growth, outgrowing the others. The rods or lamellae of the central grain or grains adopted an orientation between these extremes as shown in the schematic of Figure 25.

These results suggest that in this region, the liquid-solid interface (assuming it can be delineated by constructing perpendicular to the lamellae) adopts a concave downwards shape. For  $\theta > 8^\circ$ , no multiple grain structure developed and the rods and lamellae tended to align themselves parallel to the insert wall, such that the liquid-solid interface was perpendicular to it.

(3) Abrupt Changes in Growth Direction with Constant Cross-Section

These observations relate to the central portion of insert (a) in Figure 1.

From experiments in which growth was terminated within the upper portion of the insert, the liquid-solid interface in this region remained planar and perpendicular to the insert wall regardless of the value of  $\theta$ . These results are confirmed by the observation that also in this region, in all specimens, (and for  $\theta > 8^\circ$  for all regions), the rods or lamellae grew parallel to the insert wall consistent with the suggestion of Chadwick that they grow parallel to the local heat flow path. As discussed earlier, for  $\theta > 8^\circ$  the liquid-solid interface shape would appear to be concave downward in the lower portion of insert (a).

The behavior of the structure at the bend was dependent upon  $\theta$ . For angles of  $\theta$  larger than about  $8^\circ$ , a misorientated zone was observed on the down face in the region just beyond the acute angled corner projection (Figures 26 & 27). This region corresponds to that in which the local interface movement tends to zero. It also, however, corresponds to the region in which one of the matrix grains completely outgrows its competitors, as discussed in

Section 2 and is therefore a region in which fresh nucleation must take place. On the upward face of the same specimens, i.e., in the region of the oblique angled corner, continuous rod or lamellar growth was observed. This was also true for the entire region in specimens with  $\theta < 8^\circ$  in which, at all locations, the rods or lamellae grow parallel to the insert wall.

## CONCLUSIONS TO PART II

1. Gradual convergence of the solidifying cross-section results in a decrease in the rate of solidification, i.e. the rate of movement of the composite interface with an associated increase in inter-rod or inter-lamellar spacings. Gradual divergence of the solidifying cross-section causes an equal and opposite increase in the solidification rate. For mild section variations this is not expected to seriously impair mechanical properties.
2. Gradual divergence of the solidifying cross-section at angles less than  $8^{\circ}$  cause the surface rods or lamellae to grow parallel to the diverging contour rather than the main growth direction and inter-rod or lamellar spacing decreases.
3. Gradual divergence of the solidifying cross-section at angles between  $8$  and  $20^{\circ}$  does not alter the orientation of the rods or lamellae from their initial alignment.
4. Abrupt contraction of cross-section, when accompanied by changes in growth direction  $> 8^{\circ}$  and up to  $20^{\circ}$  result in the formation of new matrix grains with lamellae or rods orientated either parallel to the original growth direction, parallel to the new growth direction or midway between these extremes the grain or grains with lamellae or rods growing in the original direction eventually dominates.
5. Abrupt contraction in cross-section accompanied by changes in growth direction  $> 8^{\circ}$  does not produce the multiple grain effect and the rods or lamellae grow parallel to the new growth direction.

6. Abrupt changes in growth direction of large angle ( $> 8^\circ$ ) give rise to lamellar or rod misorientations which can be potential areas of weakness. Deviations less than  $8^\circ$  result in continuous lamellar or rod structures parallel to the growth direction.

### PART III. THE COMPOSITION OF INTERDENDRITIC EUTECTIC

#### Binary Alloys

When cells or dendrites grow into a melt of a binary alloy the solute is rejected laterally and progressive enrichment of solute occurs in the interdendritic liquid (if  $k < 1$ ) until the eutectic composition is reached. At the eutectic temperature the remaining liquid solidifies as a two phase solid. Although the liquid composition is then at the eutectic composition, the solid which freezes out is not, and may differ substantially from it. Consider cells or dendrites of a binary alloy freezing unidirectionally as schematically shown in Figure 28. We assume that (1) equilibrium pertains at all liquid solid interfaces, (2) the effect of interface curvature on the liquidus temperature is negligible, and (3) solute diffusion in the liquid is sufficiently rapid that there is negligible undercooling in interdendritic spaces. These are the basic assumptions that have been used in recent papers in quantitative description of solute redistribution in dendritic solidification.<sup>23,24</sup> Now assume further that isotherms are planar. From assumption (3) alone isoconcentrates must also be essentially planar. Then, at any point in the liquid between the dendrites, the concentration gradient in the growth direction is given by

$$\frac{\partial C_L}{\partial x^T} = \frac{G}{m} \quad (6)$$

where  $C_L$  is liquid composition at  $x'$ , the distance in the growth direction from the eutectic isotherm.  $G$  is the temperature gradient at  $x'$  and  $m$  is the liquidus slope. A mass balance at the eutectic interface yields the equation

$$R(C_E - \bar{C}_S) = -D \left( \frac{\partial C_L}{\partial x'} \right)_{x'=0} \quad (7)$$

where  $R$  is eutectic isotherm velocity,  $C_E$  is the liquid composition at the eutectic temperature,  $\bar{C}_S$  is the average composition of the two phase solid forming at the eutectic temperature and  $D$ , the liquid diffusion coefficient.

For constant thermal gradient and liquidus slope, liquid concentration gradient is independent of  $x'$  and equations 6 and 7 can be combined to relate the average concentration of interdendritic eutectic solid ( $\bar{C}_S$ ) to the solidification variables,

$$(C_E - \bar{C}_S) = - \frac{DG}{Rm} \quad (8)$$

For negative  $m$  (hypoeutectic alloys),  $\bar{C}_S$  is always less than  $C_E$ , approaching  $C_E$  as a limit at very low values of  $G/R$ . At the other limit  $\bar{C}_S$  approaches  $C_0$ . At this limit, at steady state, conservation of solute requires that there be no primary dendrites present; i.e., that the structure be entirely a two phase composite. This same conclusion is reached by re-writing equation (3) with  $\bar{C}_S = C_0$  in the following form:

$$G/R = \frac{(C_E - C_0) m}{D} \quad (9)$$

Equation 9 is exactly the critical condition for stability of a plane front in a two-phase alloy (Mollard and Flemings<sup>2</sup>-- equation (4)). Both equations (8) and (9) assume constitutional supercooling in front of the two-phase interface which is exactly zero, and both equations give the required G/R to achieve this. Equation (8) applies to the interdendritic eutectic in dendritic solidification and equation (9) to a fully plane interface.

The usual way of comparing the stability equation (9) with experiment is to perform a series of experiments at constant  $C_0$ , varying G/R. A critical value of G/R is ultimately bracketed, below which the structure obtained is cellular or dendritic and above which it is planar. Comparison of equations (8) and (9) suggests a simpler way of accomplishing this. Imagine a series of experiments conducted at a given constant G/R such that a dendritic structure is obtained. Composition of the alloys studied,  $C_0$ , is varied from  $C_E$  to  $C_0$ , the critical composition at which a plane front is obtained according to equation (9). Now, in all these experiments the composition of the interdendritic two-phase material is a constant,  $\bar{C}_S$ , as given by equation (8). Furthermore, the composition is exactly equal to  $C_0$ , the critical composition at which a plane front would be obtained with the given G/R. Thus, measurement of  $\bar{C}_S$  in a dendritically solidified alloy gives directly the critical composition for stability of a plane front at the given G/R. This simplified method of determining interface stability has the advantage of requiring only a single experiment to obtain the critical value of G/R.

### Ternary Alloys

Exactly similar considerations apply to ternary as to binary alloys. Consider, as example, an alloy such as alloy  $C_0$  from the ternary system sketched in Figure 29a. In the general case, the solid first forms as a primary single phase as sketched in Figure 29b. Then, except at very high  $G/R$ , the interdendritic liquid composition is enriched to that of a line of two-fold saturation, at which time two phases form simultaneously as also sketched in Figure 29b. The variation of  $C_{Lm}$  with  $C_{Ln}$  as  $x'$  is varied from 0 to  $x'_t$  is termed the "solidification path." This is shown schematically by the line  $C_t - C_{2t} - C_E$  in Figure 29a. Following exactly the assumptions used to describe the binary alloy case, we can relate concentration gradient to temperature gradient for each minor component in equations analogous to equation (6). These are applicable in the liquid between the two-phase dendrites;

$$\frac{\partial D_{Lm}}{\partial x'} = \frac{G}{m_{em}} \quad (10a)$$

$$\frac{\partial C_{Ln}}{\partial x'} = \frac{G}{m_{en}} \quad (10b)$$

$C_{Lm}$ ,  $C_{Ln}$  are liquid compositions in components m and n at position  $x'$ .  $m_{em}$  and  $m_{en}$  are the slopes of the line of two-fold saturation in terms of components m and n respectively at the given compositions. Setting up a mass balance at the eutectic interface for each component, assuming the off-diagonal diffusion coefficients negligible,

$$R (C_{Em} - \bar{C}_{Sm}) = -D_m \frac{\partial C_{Lm}}{\partial x'} \quad (11a)$$

$$x'=0$$

$$R (C_{En} - \bar{C}_{Sn}) = -D_n \frac{\partial C_{Ln}}{\partial x'} \quad (11b)$$

$$x'=0$$

Where  $\bar{C}_{Sm}$ ,  $\bar{C}_{Sn}$  are the average concentrations of the interdendritic eutectic in the two components,  $C_{Em}$ ,  $C_{En}$  are the concentrations of m and n in the ternary eutectic.  $D_m$ ,  $D_n$  are the liquid diffusion coefficients. Combining equations (10) and (11) for constant G and constant liquidus slopes gives the results,

$$(C_{Em} - \bar{C}_{Sm}) = \frac{-D_m}{m_{em}} (G/R) \quad (12a)$$

$$(C_{En} - \bar{C}_{Sn}) = \frac{-D_n}{m_{en}} (G/R) \quad (12b)$$

These equations predict the difference between the eutectic composition and the average interdendritic solid composition for each of the minor components as a function of G/R.

We shall show now, that these are equivalent to the equations obtained for the stability of the "maximum stability" alloys of Rinaldi et al.<sup>3</sup> Maximum stability alloys were described as those alloys which, when solidified with plane front have diffusion paths which approach the ternary eutectic along the line of two-fold saturation. A diffusion path is shown schematically by the dashed

line  $C_O-C_E$  in Figure 29a. For maximum stability alloys, the stability expression (Rinaldi et al, equation (11)) can be written for two liquidus surfaces, since both phases are in equilibrium at the same time.

$$G/R \geq P_1 \frac{(C_{Em} - C_{Om})}{D_m} + s_1 \frac{(C_{En} - C_{On})}{D_n} \quad (13a)$$

$$G/R \geq P_2 \frac{(C_{Em} - C_{Om})}{D_m} + s_2 \frac{(C_{En} - C_{On})}{D_n} \quad (13b)$$

$P_1, s_1, P_2, s_2$  are the liquidus slopes of the two components for the two liquidus surfaces, defined as:

$$P_1 = \left( \frac{\partial T_L}{\partial C_{Lm}} \right)_1 \quad P_2 = \left( \frac{\partial T_L}{\partial C_{Lm}} \right)_2$$

$$s_1 = \left( \frac{\partial T_L}{\partial C_{Ln}} \right)_1 \quad s_2 = \left( \frac{\partial T_L}{\partial C_{Ln}} \right)_2$$

where  $T_L$  is the equilibrium liquidus temperature. Combining 13a and 13b and re-arranging

$$G/R \geq \left( \frac{P_1 s_2 - P_2 s_1}{s_2 - s_1} \right) \frac{C_{Em} - C_{Om}}{D_m} \quad (14)$$

From the geometry of the intersecting planes in the phase diagram

$$m_{em} = \left( \frac{P_1 s_2 - P_2 s_1}{s_2 - s_1} \right) \quad (15)$$

where  $m_{em}$  is the slope of the line of two-fold saturation in terms of component m. Substituting this into equation 13, the stability equation simplifies to:

$$G/R \geq m_{em} \left( \frac{C_{Em} - C_{Om}}{D_m} \right) \quad (16)$$

A similar equation can be written in terms of component n.

Comparing equations (12) and (15), we note again the equivalency in considering the stability of the planar, three phase interface with the stability of the interdendritic eutectic front. We conclude that for a particular set of growth conditions the composition of the interdendritic eutectic in a ternary alloy, whose dendrites are two-phase over at least part of their length, is the same as that of the maximum stability alloy which would just be stable under those growth conditions.

#### Experimental Apparatus and Procedure

Experimental verification of the ideas outlined above was obtained using binary Al-Cu alloys and ternary Al-Cu-Ni alloys. Relevant portions of the phase diagrams for these systems are as shown schematically in Figures 28a and 29a respectively. The apparatus and method for producing specimens grown were as reported by Rinaldi et al. <sup>3</sup>

Microanalysis was carried out on an ARL microprobe using a 30 KV accelerating potential. A beam size of the order of 20  $\mu$ m was employed in order to average over the two or three phases in the interdendritic eutectic. Because of the necessity of averaging over

an inhomogeneous solid, it was decided not to attempt to use theoretical methods for the calculation of correction factors. Three two-phase standards were used covering the range of alloy compositions studied. A smooth curve was drawn through the results for the standards and this curve used to correlate X-ray intensity ratios with composition in weight percent. The compositions of the three standards were determined by wet chemical analysis. These and the ratio of intensities on the standards to those on pure copper are given below:

<u>Wt. % Cu</u>	<u>Intensity Ratio</u>
19.1	27.5
33.9	31.5
38.5	37.2

In the specimens investigated, CuK X-ray counts were taken in the interdendritic eutectic. Counts for ten seconds were made and twenty such readings taken. No analysis was made for nickel in the ternary system because the percentage of nickel in the ternary eutectic is small (0.4 at %) and it is therefore time consuming to determine quantitatively using electron microprobe analysis.

#### Results and Discussion

Specimens of four initial compositions were prepared, two in the binary Al-Cu system and two in the ternary Al-Cu-Ni system. These compositions are listed in Table IV divided into three groups-- hypoeutectic binary, hypereutectic binary and ternary. Also listed are the growth conditions used for the solidification of each specimen. All specimens had dendritic or cellular microstructures of the type shown by Rinaldi et al.<sup>3</sup> All but two of the alloys

from the ternary system also possessed two-phase cells or dendrites. Compositions of the interdendritic eutectic as determined by microprobe analysis were plotted against the function G/R. Results are shown in Figures 30 and 31. Points plotted represent all the data in Table IV except from runs of the ternary alloy where only single-phase cells or dendrites were obtained. This case is not covered by the analysis presented.

Figure 30 containing the results for the binary system, also shows the theoretical line as calculated from equation (8) using a value of  $3.25 \times 10^{-5} \text{ cm}^2/\text{sec}$  for the diffusion coefficient<sup>24</sup> and values of  $m$  obtained from the phase diagram, viz:

$$m_{\text{Al}} = 6.5^\circ\text{C/at}\% \quad m_{\text{CuAl}_2} = 5.1^\circ\text{C/at}\%$$

It can be seen from the figure that average interdendritic eutectic compositions are not equal to the eutectic composition, but differ by amounts which depend on G/R. This is also seen on Figure 31 where the theoretical relation between  $\bar{C}_g$  and G/R is calculated from equation (12) using the following constants.<sup>3</sup>

$$D_{\text{Cu}} = 1.9 \times 10^{-5} \text{ cm}^2/\text{sec} \quad m_{\text{em}} = 4.58^\circ\text{C/at}\%$$

$$D_{\text{Ni}} = 1.7 \times 10^{-5} \text{ cm}^2/\text{sec} \quad m_{\text{en}} = 23.30^\circ\text{C/at}\%$$

Figure 30 also shows the experimental results of Jordan and Hunt<sup>24</sup> for the eutectic/dendritic transition in the Al-CuAl<sub>2</sub> system. The experimental points for the interdendritic eutectic composition fall more closely on to these experimental lines for the eutectic/dendritic transition than on to the line representing

equation (8). Apparently, the same approximations inherent in the Mollard and Flemings analysis are also inherent in the derivation of equation (8). An important conclusion to be drawn from Figure 30 is that measurement of interdendritic "eutectic" composition provides a simple method of determining the stability of composite structures. The determination can be done with many fewer specimens than has previously been required, since each specimen gives a point on the curve. The accuracy of determination is shown here to be equal to that obtained by the earlier method.

Turning to the ternary system, we have already noted that good agreement exists between the experimental results and the theoretical line for alloys of maximum stability. Our experimental results are also compared in Figure 4 with the results of Rinaldi et al <sup>3</sup> for alloys on the line of two-fold saturation. Alloys on this line are not far from those on the line of maximum stability. Thus, G/R for stability of these alloys should be close to, but above, that for alloys on the line of two-fold saturation. This is the result obtained in Figure 31 for alloys several percent or more removed from the eutectic. For alloys closer to the eutectic the several curves and data are essentially equivalent.

### CONCLUSIONS TO PART III

1. A theory has been developed which relates the composition of interdendritic "eutectic" in unidirectional solidification to solidification variables. The theory predicts that this composition should be not equal to the true eutectic composition, but tend towards it at low values of  $G/R$ .
2. The theory predicts that in binary alloys the composition of interdendritic eutectic is exactly equivalent to the composition of that alloy which would just grow with a plane front at equivalent value of  $G/R$ . In ternary alloys it is equivalent to that of the "maximum stability" alloy that would just grow with a plane front at equivalent  $G/R$ .
3. The theory was tested on Al-Cu binary alloys and on the Al-Cu-Ni ternary alloys. In all specimens the composition of interdendritic eutectic was not equal to the eutectic composition.
4. Experimental values of  $G/R$  for stability determined by the new method described herein are close to those obtained by the method used previously. The new method has the advantage of greater simplicity. In ternary alloys it also provides information directly as to which alloys are those of maximum stability.

## APPENDIX A

### Analysis of Electron Microprobe Data

In order to apply equation (2) to the aluminum-copper-nickel ternary system, it is necessary to obtain numerical values for  $D_{Cu}$ ,  $D_{Ni}$ , and  $k_m$ . This was done by the procedure outlined by Sharp and Hellowell.<sup>12</sup> The composition profile measured ahead of the quenched interfaces of ingots numbers 1, 11 and 19 with an electron beam microanalyzer. A 25 micron round spot was used in order to average over fine microsegregation in the quenched liquid. The background level was approximately five counts per second.

The data obtained are shown in Figures 11 and 12. A semi-logarithmic plot of  $C_L - \bar{C}_S$  (C.P.S.) versus distance was used for copper (Figure 13) and for nickel (Figure 14).

The difference in correction factor for the range of copper concentration encountered was sufficiently small that, within that range ratios of counts per second could be treated as ratios of concentration. As outlined by Sharp<sup>12</sup> in the aluminum-copper system with up to 20% Cu,

$$\frac{I_A}{\frac{I(A)}{C_A}} = .8935 + .1 C_A \quad (17)$$

where  $C_A$  is the weight fraction of the alloying element added and  $I_A/I(A)$  is the intensity ratio of the specimen's radiation to that of a 100% standard. Therefore, for 1% Cu

$$\frac{I_A/I(A)}{C_A} = .8945$$

and for 6% Cu

$$\frac{I_A/I(A)}{C_A} = .8995$$

So the maximum error introduced by counts per second in place of weight percent is

$$\text{Error} = \frac{.8995 - .8945}{\frac{.8995 + .8945}{2}} = \frac{.005}{.8970} = 5.6 \times 10^{-2} \text{ or } .56\%$$

Since

$$\frac{C_L - C_O}{C_L^* - C_O} = e^{-\frac{R}{D} x}$$

values of  $D_{Ni} = 1.74 \times 10^{-5} \text{ cm}^2/\text{sec}$  and  $D_{Cu} = 3.25 \times 10^{-5} \text{ cm}^2/\text{sec}$  were obtained from the slopes of Figures 13 and 14. From Figure 15 it was found that

$$\bar{k}_m = .189$$

<u>Ingot No.</u>	<u><math>\bar{k}_m</math></u>
1	.189
11	.183
19	.196
Average	.189

## APPENDIX B

### Determination of $p$ , $s$ , $C_{Ln}$ , $C_{Lm}$ , and the Stability Criterion From the Al-Cu-Ni Diagram

#### Determination of $p$ and $s$ from the Liquid Surface

The liquidus surface was approximated by the following points on the  $\alpha$  side.

	$C_{Lm}$ (wt pct Cu)	$C_{Ln}$ (wt pct Ni)	$T_L$ ( $^{\circ}C$ )	reference
1.	0	0	660	14,15
along the line of two-fold saturation:				
2.	0	5.7	640	15
3.	14.1	4.7	599	16
and on the $\epsilon$ side:				
4.	1	9.0	700	14

A vector treatment was used to obtain the equation of the liquidus. The notation  $\bar{V}_{a,b}$  is used to denote a vector from points a to b. For the liquidus surface on the  $\alpha$  side of the line of twofold saturation:

$$\bar{V}_{1,2} = 0\mathbf{i} + 5.7\mathbf{j} - 20\mathbf{k}$$

$$\bar{V}_{3,2} = -14.1\mathbf{i} + 1\mathbf{j} + 41\mathbf{k}$$

where  $\mathbf{i}$ ,  $\mathbf{j}$  and  $\mathbf{k}$  are orthogonal unit vectors located respectively along the  $C_{Lm}$ ,  $C_{Ln}$  and  $T$  axes.

$$\bar{N} = \bar{V}_{1,2} \times \bar{V}_{3,2} = \begin{vmatrix} \mathbf{i} & \mathbf{j} & \mathbf{k} \\ 0 & 5.7 & -20 \\ -14.1 & 1 & 41 \end{vmatrix}$$

$$\bar{N} = 253\mathbf{i} + 280\mathbf{j} + 80\mathbf{k}$$

The equation of the plane is, therefore,

$$253C_{Lm} + 280C_{Ln} + 80T_L = D$$

where

$C_{Lm}$  = copper concentration in wt pct Cu

$C_{Ln}$  = nickel concentration in wt pct Ni

$T_L$  = liquidus temperature in  $^{\circ}\text{C}$

Substituting (0, 0, 660) yields

$$D = 52,800$$

$$T_L = 660 - 3.5C_{Ln} - 3.16C_{Lm} \quad (18)$$

$$p = \frac{\partial T_L}{\partial C_{Lm}} = -3.16$$

$$s = \frac{\partial T_L}{\partial C_{Ln}} = -3.5$$

where  $C_{Lm}$  and  $C_{Ln}$  are the concentrations of Cu and Ni respectively in the liquid.

For the liquidus surface on the  $\epsilon$  side:

$$\bar{V}_{2,4} = 1\mathbf{i} + 3.3\mathbf{j} + 60\mathbf{k}$$

$$\bar{V}_{3,4} = -13.1\mathbf{i} + 4.3\mathbf{j} + 101\mathbf{k}$$

$$\bar{N} = \bar{V}_{2,4} \times \bar{V}_{3,4} =$$

i	j	k
1	3.3	60
-13.1	4.3	101

$$\bar{N} = 75\mathbf{i} - 887\mathbf{j} + 47.5\mathbf{k}$$

$$\therefore 75C_{Lm} - 887C_{Ln} + 47.5T = D$$

Substituting (0, 5.7, 640)

$$D = 25,344$$

$$T_L = 534 + 18.6C_{Ln} - 1.58C_{Lm} \quad (19)$$

$$p = \frac{\partial T_L}{\partial C_{Lm}} = -1.58$$

$$s = \frac{\partial T_L}{\partial C_{Ln}} = 18.6$$

### Determination of the Solidus Surface

The solidus surface was approximated by the following points:

	$C_{Sm}$ (wt pct Cu)	$C_{Sn}$ (wt pct Ni)	$T_S$ ( $^{\circ}C$ )	References
1.	1.7	0	599	16
2.	1.0	42	599	16
3.	0	5.7	640	15

$$\bar{V}_{1,2} = -0.7\bar{i} + 42\bar{j} + 0\bar{k}$$

$$\bar{V}_{1,3} = -1.7\bar{i} + 5.7\bar{j} + 41\bar{k}$$

$$\bar{N}_s = \bar{V}_{1,2} \times \bar{V}_{1,3} = \begin{vmatrix} \bar{i} & \bar{j} & \bar{k} \\ -0.7 & 42 & 0 \\ -1.7 & 5.7 & 41 \end{vmatrix}$$

$$\bar{N}_s = 1620\bar{i} + 28.6\bar{j} + 67.5\bar{k}$$

$$\therefore 1620C_{Sm} + 28.6C_{Sn} + 67.5T_S = D$$

Substituting (0, 5.7, 640) yields

$$D = 43,362 \quad (20)$$

$$T_S = 642 - .412C_{Sn} - 24.0C_{Sm}$$

### Determination of the Line of Twofold Saturation

The line of twofold saturation was approximated from the following points:

	$C_{Lm}$ (wt%Cu)	$C_{Ln}$ (wt%Ni)	$T_L(^{\circ}C)$	<u>Reference</u>
1.	0	5.7	640	15
2.	14.1	4.7	599	16

$$\bar{V}_{1,2} = (14.1-0)\underline{i} + (4.7-5.7)\underline{j} + (599 - 640)\underline{k}$$

$$\bar{V}_{1,2} = 14.1\underline{i} - 1.0\underline{j} - 41\underline{k}$$

The equation of the line in the direction of  $\bar{V}_{1,2}$  passing through the point (0, 517, 640) is:

$$\frac{C_{Lm}}{14.1} = \frac{(C_{Ln} - 5.7)}{-1} = \frac{T_L - 640}{-41} \quad (21)$$

### Determination of the Stability Criteria

Method I - This is based on an approximate model for the liquidus surfaces, solidus surface and the line of two-fold saturation.

Using relationships derived earlier in this appendix, values of the stability criterion are obtained. These values are plotted in Figure 9.

Method II - This modifies Method I and is based on electron microprobe data.

It was established from electron microprobe data in appendix A that  $\bar{k}_m = .189$  for ingot no. 1. Referring to the 600°C isotherm

through the Al-Cu-Ni system given in Figure 15, it is seen that the copper content at the solidus is constant. Therefore, the value,  $\bar{k}_m = .189$  should be valid for the range of nickel composition considered. Since all of the specimens were of approximately 1 wt% Cu and  $\bar{k}_m = \bar{C}_{Sm}/C_{Lm}^* = .189$ , the liquidus composition,  $C_{Lm}^*$ , must be approximately 5.3 wt%. Since, in composite growth, two phases solidify simultaneously,  $C_{Lm}^*$  and  $C_{Ln}^*$  must be on the line of two-fold saturation. Referring to equation (21),  $C_{Ln}^*$  and  $T_L$  are obtained:

$$\frac{C_{Lm}^*}{14.1} = \frac{C_{Ln}^* - 5.7}{-1} = \frac{T_L - 640}{-41}$$

$$C_{Ln}^* = 5.32$$

$$T_L = 625.7$$

Substituting into equation 2, the following is obtained:

$$\begin{aligned} &\text{for } C_{On} < 5.5 \text{ wt\%Ni} \\ &G/R \geq 4.16 \times 10^5 + 2.01 \times 10^5 (5.3 - C_{On}) \end{aligned} \quad (22)$$

$$\begin{aligned} &\text{for } C_{On} > 5.5 \text{ wt\%Ni} \\ &G/R \geq 1.28 - 10.6 \times 10^5 (5.3 - C_{On}) \end{aligned} \quad (23)$$

Table I  
Specimens (Part I)

<u>ingot no.</u>	<u>C<sub>0n</sub> wt % Ni</u>	<u>C<sub>0m</sub> wt % Cu</u>	<u>G °C/cm</u>	<u>R cm/hr</u>	<u>G/Rx10<sup>-5</sup> °C-sec/cm<sup>2</sup></u>	<u>Structure</u>
1	3.92	1.11	113	.625	6.5	VI
2			143	1.07	4.8	III
			176	6.0	1.06	I
4	5.02	.82	170	1.0	6.1	VI
5			185	3.4	1.95	II
6			180	1.6	4.05	II
7			264	3.4	2.8	II
8			188	.75	9.0	VI
9			200	3.36	2.4	II
10			185	6.7	.995	II
11	5.15	.95	132	.98	4.85	VI
12			126	2.35	1.95	V
13			203	5.2	1.40	V
14			213	6.0	1.28	V
15			140	6.0	.85	V
16			127	6.5	.71	V
17			179	6.0	1.05	V
18			157	1.5	3.78	VI
19	6.0	1.01	154	.9	6.03	VI
20			171	1.51	4.1	II
21			169	3.13	1.94	II
22	7.3	.92	137	.6	7.6	IV
23			151	1.66	3.26	II
24			132	.355	13.4	IV
25			284	.4	25.5	IV
25	8.85	.92	.58	.56	10.5	IV

Structure Types

- I- Aligned single-phase dendrites, aligned two-phase cells, and aligned three-phase composite.
- II- Aligned single-phase cells, aligned two-phase cells, and aligned three-phase composite.
- III- Aligned single-phase dendrite and aligned two-phase composite.
- IV- Aligned single-phase cells and aligned two-phase composite.
- V- Aligned two-phase cells and aligned three-phase composite.
- VI- Aligned two-phase composite.

Table II

Specimens from High Thermal Gradient Apparatus (Part I)

Ingot #	$C_{OM}$ wt%Ni	$C_{Om}$ wt%Cu	G $^{\circ}C/cm$	R cm/hr	$G/R \times 10^{-5}$ $^{\circ}C\text{-sec}/cm^2$	Structures
1A	6.54	.99	475	.353	48	VI
2A	6.54	.99	344	.424	30	VI
3A	6.54	.99	358	.5	26	VI
4A	6.54	.99	286	.82	13	VI
5A	6.54	.99	345	1.28	10	VI
6A	6.54	.99	430	1.74	9	VI
7A	6.54	.99	300	2.52	4	V
8A	7.3	1.08	500	.6	30	VI
9A	7.3	1.08	590	.81	26	VI
10A	7.3	1.08	400	1.08	13	IV
11A	7.3	1.08	360	2.11	6	II
12A	8	1	460	.54	31	VI

Structure Types

- I - Aligned single-phase dendrites, aligned two-phase cells, and aligned three-phase composite.
- II - Aligned single-phase cells, aligned two-phase cells, and aligned three-phase composite.
- III - Aligned single-phase dendrite and aligned two-phase composite.
- IV - Aligned single-phase cells and aligned two-phase composite.
- V - Aligned two-phase cells and aligned three-phase composite.
- VI - Aligned two-phase composite.

Table III

Operational Parameters of Runs 0002-0021 (Part II)

Sample Number	Alloy	Angle $\theta$	Rate cm/hr	Gradient $^{\circ}\text{C/cm}$	G/R $10^{-5} \text{ } ^{\circ}\text{C}\cdot\text{sec/cm}^2$
0002	Al-6.1%Ni	$14^{\circ}$			
0003	Al-6.1%Ni	$14^{\circ}$	.75	235	11.3
0004	Al-6.1%Ni	$14^{\circ}$	1.83	278	5.47
0005	Al-6.1%Ni	$14^{\circ}$	2.73	310	4.08
0006	Al-6.1%Ni	$18^{\circ}$	1.85	270	5.46
0007	Al-6.1%Ni	$18^{\circ}$	2.02	-	-
0008	Al-6.1%Ni	$18^{\circ}$	1.15	255	8.0
0009	Al-.73%Ni- 32.94%Cu	$18^{\circ}$	1.20	342	10.3
0010	"	$16^{\circ}$	1.20	273	8.2
0011	"	$20^{\circ}$	1.20	276	8.27
0012	"	$20^{\circ}$	2.22	276	4.5
0013	"	$14^{\circ}$	1.2	400	12.0
0014	"	$10^{\circ}$	2.0	350	6.3
0015	"	$6^{\circ}$	1.2	375	11.0
0016	"	$14^{\circ}$	2.2	375	6.0
0017	"	$6^{\circ}$	1.8	330	6.6
0018	"	$8^{\circ}$	1.2	342	10.3
0019	"	$12^{\circ}$	1.2	342	10.0
0020	"	$12^{\circ}$	2.0	334	6.0
0021	"	$8^{\circ}$	2.2	230	3.76

Table IV  
Details of Solidification Conditions  
and Results Obtained (Part III)

	G $\frac{^{\circ}\text{C}}{\text{cm}}$	R $\frac{\text{cms}}{\text{sec}} \times 10^4$	GR $\frac{^{\circ}\text{C}}{\text{sec}} \text{cm}^{-2} \times 10^{-6}$	$C_s$ at %Cu	two-phase dendrites present	
Binary-hypoeutectic $C_o = 9.09$ at %Cu	176	5.50	0.32	14.7		
	191	2.62	0.73	13.35		
	187	2.26	0.83	13.6		
	184	1.07	1.72	11.4		
	288	0.86	3.37	9.1		
Binary - hypereutectic $C_o = 21.2$ at %Cu	176	5.35	0.33	18.6		
	157	1.46	1.08	20.4		
	160	0.93	1.71	21.2		
Ternary	$C_{om} = 14.3$ at %Cu	182	5.43	0.34	15.4	yes
	$C_{on} = 0.94$ at %Ni	192	3.04	0.63	14.6	yes
		238	2.53	0.94	14.7	no
	$C_{om} = 12.3$ at %Cu	342	2.70	1.29	12.4	yes
	$C_{on} = 1.32$ at %Ni	270	1.60	1.69	11.2	yes
	294	1.41	2.09	10.9	no	

#### REFERENCES

1. H. Bibring, M. Rabinovitch, G. Seibel, *Comptes Rendue*, Vol. 268 (1969) 1966.
2. F. R. Mollard, M. C. Flemings, *Trans. AIME* Vol. 239 (1967) 1526.
3. M. D. Rinaldi, R. M. Sharp, M. C. Flemings, *Met. Trans.* Vol. 3 (1972) 3133.
4. J. D. Hunt, J. P. Chilton, *J.I.M.* Vol. 91 (1962-63) 338.
5. J. D. Hunt, J. P. Chilton, *J.I.M.* Vol. 92 (1963-64) 21.
6. D. Jaffrey, G. A. Chadwick, *Phil. Mag.* Vol. 18 (1968) 573.
7. D. Jaffrey, G. A. Chadwick, *J.I.M.* Vol. 97 (1969) 118.
8. D. Jaffrey, G. A. Chadwick, *Met. Trans.* Vol. 1 (1970) 3389.
9. P. M. Curran, J. S. Erickson, *Third Quarterly Report* (1974 Jan.) Contract N00019-73-C-0252.
10. M. M. Farag, M. C. Flemings, to be published.
11. M. D. Rinaldi, R. M. Sharp, M. C. Flemings, *Technical Report AFML-TR-72-161*.
12. R. M. Sharp, A. Hellawell, *J. Cryst. Growth*, Vol. 5 (1969) 155.
13. *Aluminum* Vol. 1 ASM, Ohio (1972).
14. W. Koster, U. Zwicker, K. Moeller, *Z. Metallkund*, Vol. 39 (1948) 225.
15. M. Hansen, *Constitution of Binary Alloys*, McGraw-Hill, New York (1958).
16. H. Hannemann, A. Schrader, *Atlas Metallagraphicus* Vol. III (1952).
17. G. A. Chadwick, *J.I.M.* Vol. 91 (1963) 298.
18. R. W. Hertzberg, F. D. Lemkey, J. A. Ford, *Trans. AIME* Vol. 233 (1965) 347.

19. E. E. Underwood, Quantitative Stereology, Addison Wesley  
(1970) 73-75.
20. G. A. Chadwick, I.S.I. publ. 110 (1968) 138.
21. G. A. Chadwick, J.I.M. Vol. 92 (1963-64) 18.
22. H. D. Brody, M. C. Flemings, Trans. AIME Vol. 236 (1966) 615.
23. M. C. Flemings, G. E. Nereo, Trans. AIME Vol. 239 (1967) 1449.
24. R. M. Jordan, J. D. Hunt, Met. Trans. Vol. 2 (1971) 3401.

$\alpha$ : Al Solid Sol.  
 $\epsilon$ : NiAl<sub>3</sub>  
 $\delta$ : Ni<sub>2</sub>Al<sub>3</sub>  
 $\tau$ : Cu<sub>3</sub>NiAl<sub>6</sub>  
 $\theta$ : CuAl<sub>2</sub>

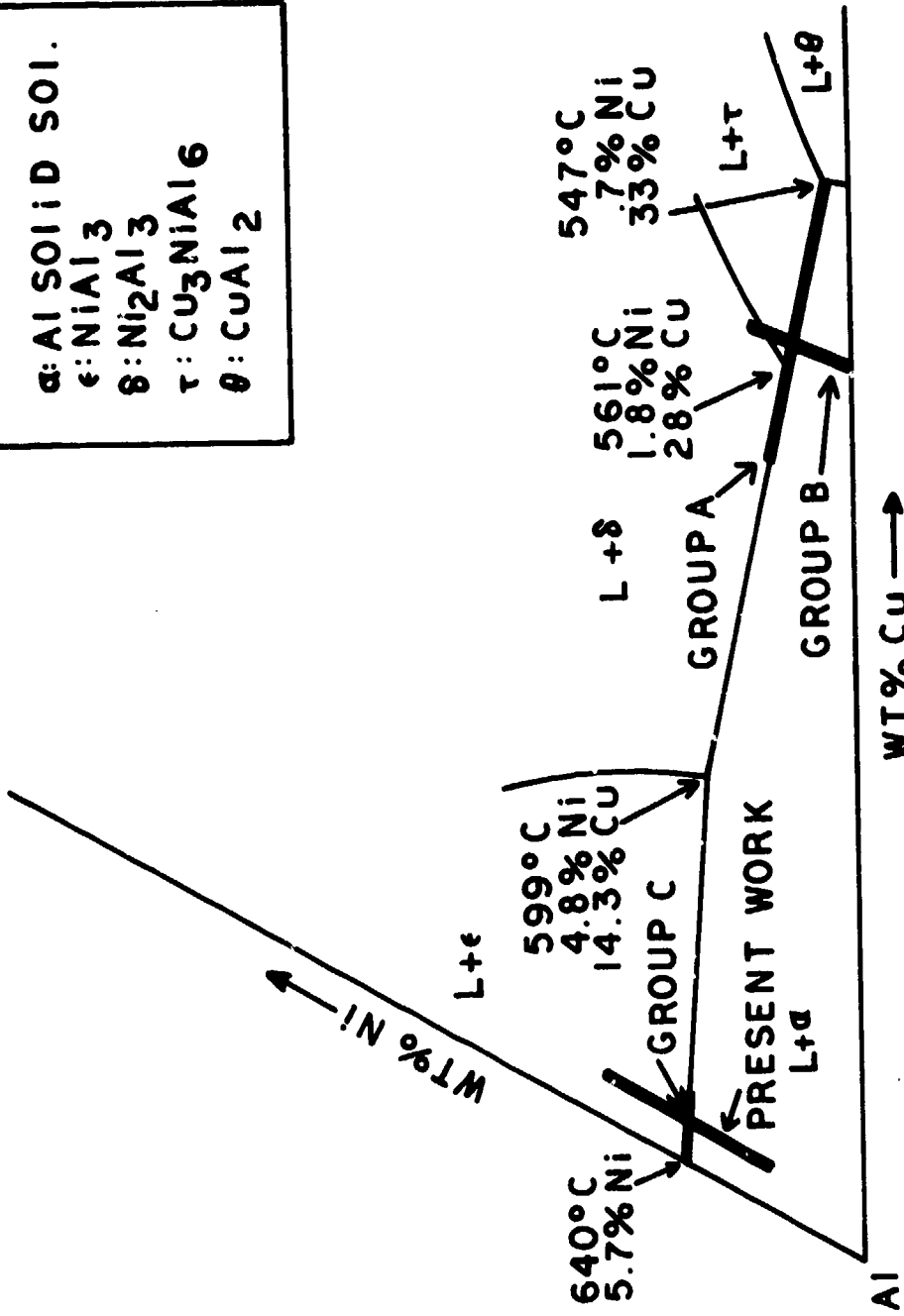


Figure 1. Composition ranges of specimens used by Rinaldi et al and the present work. (Ternary section from ref. 14.)

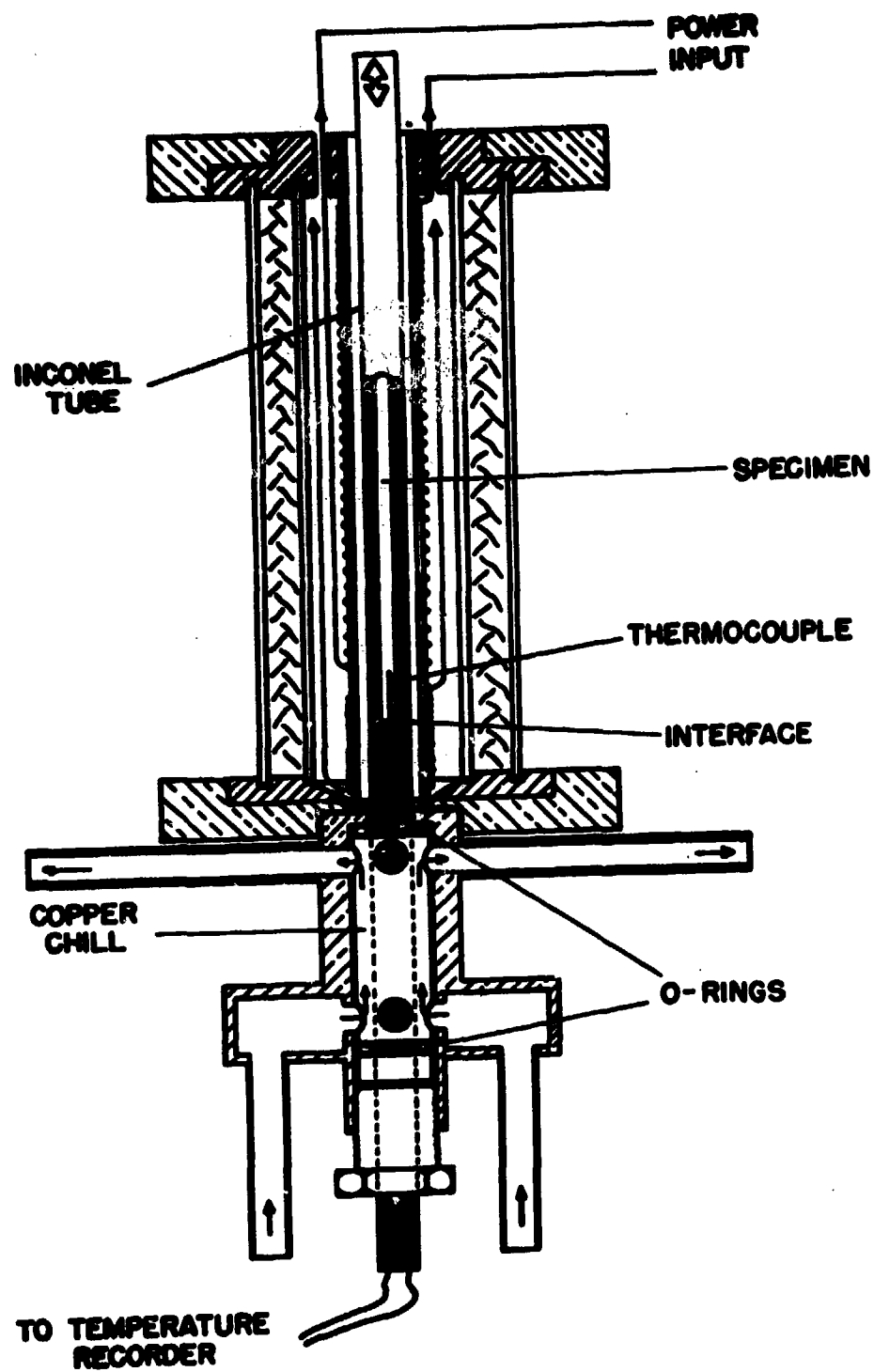


Figure 2. Schematic representation of the furnace-chill assembly of the apparatus used by Rinaldi et al.

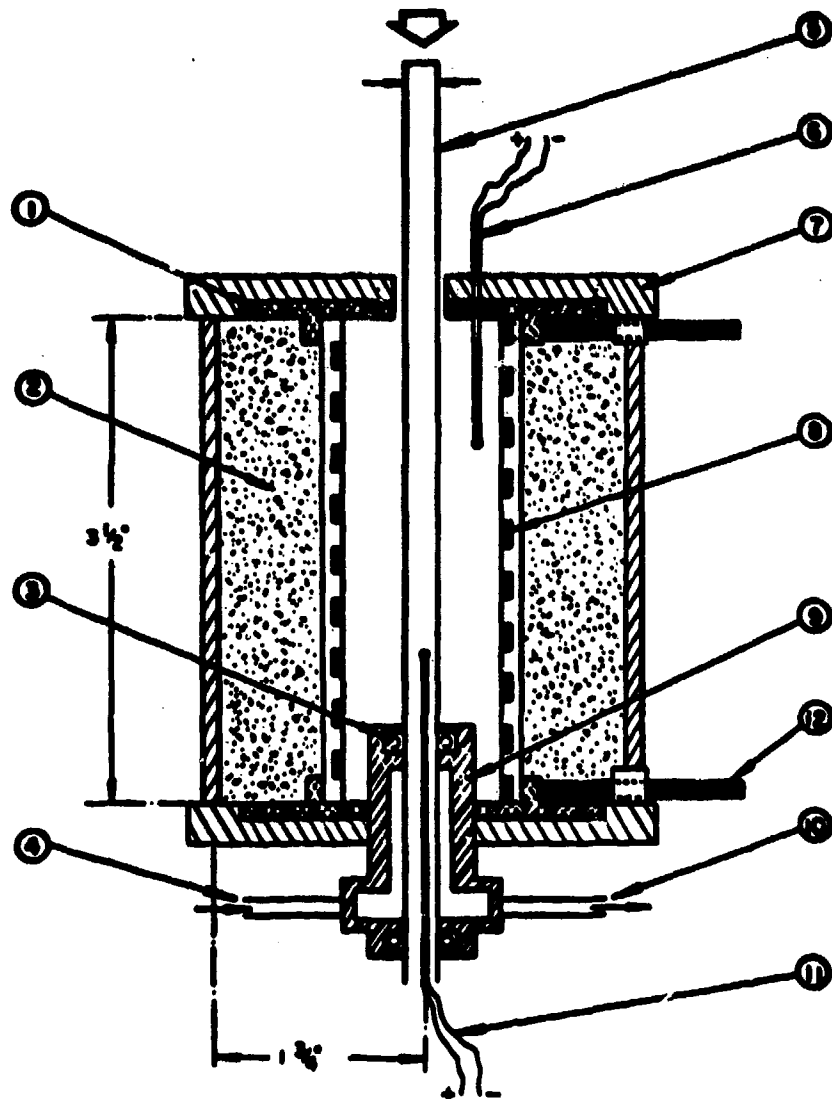
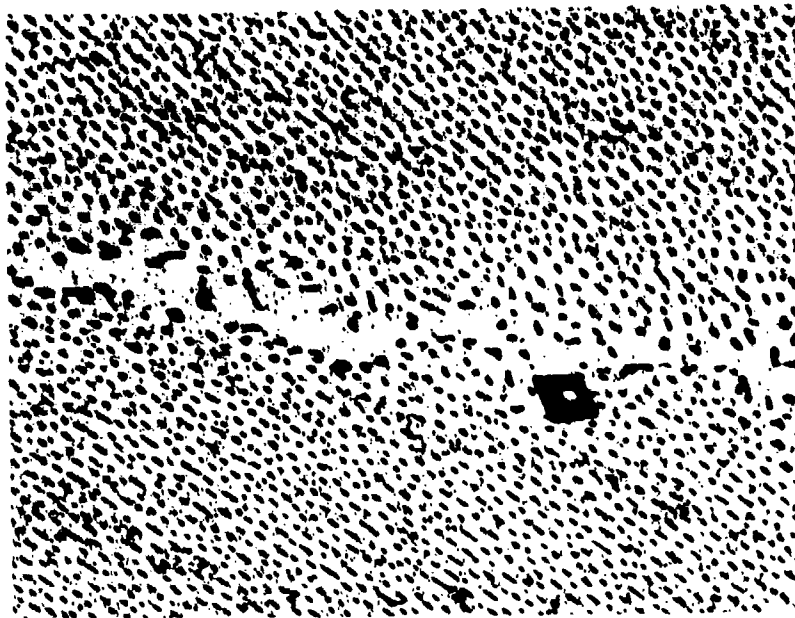
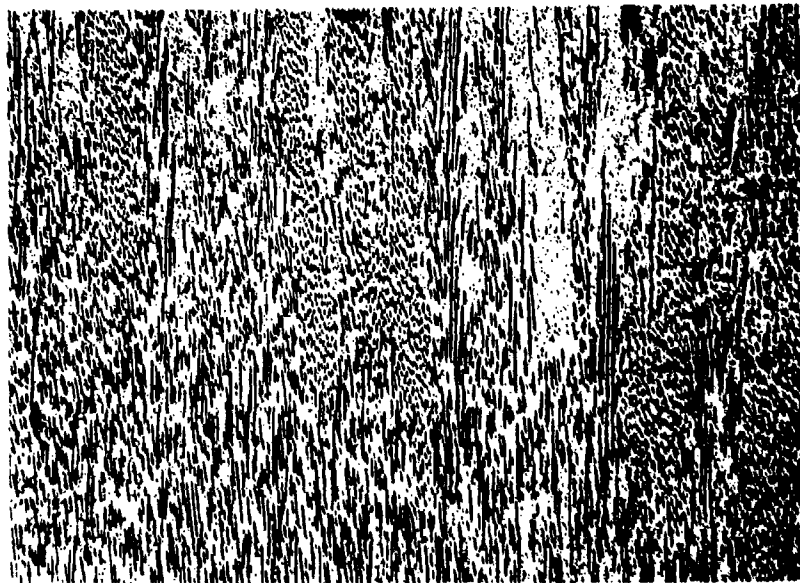


Figure 3. High gradient crystal growth apparatus. (1) Lava plug, (2) Fiberfrax insulation, (3) Viton O-ring, (4) coolant water in, (5) alumina crucible  $\frac{1}{4}$  in. diameter, (6) furnace thermocouple, (7) stainless steel housing, (8) platinum-rhodium heating strip, inside wound, .010"x.0625", (9) brass chill chamber, (10) coolant water out, (11) specimen thermocouple, (12) element electrical connection.

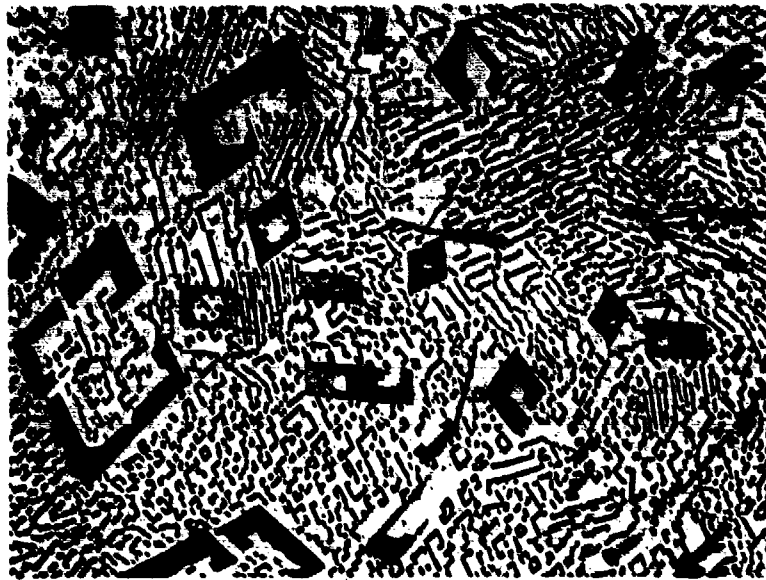


(a)

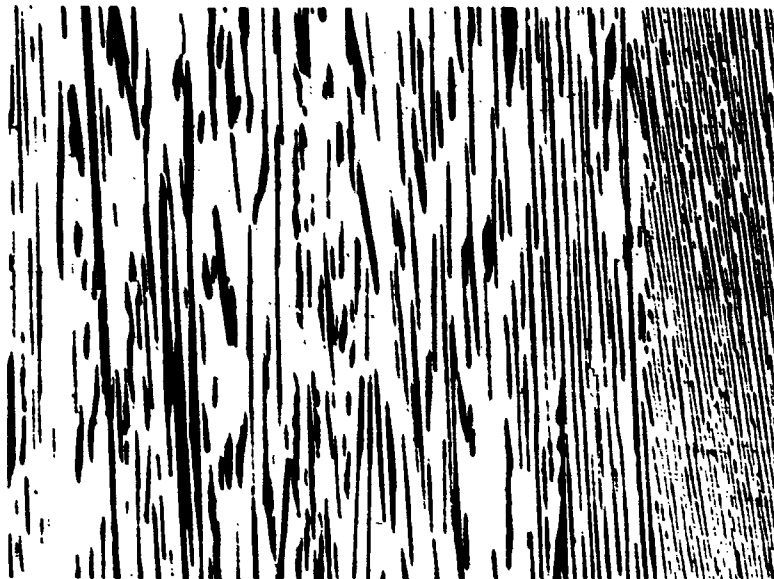


(b)

Figure 4. Ingot #20, 6.0 wt% Ni, 1.01 wt% Cu,  $G/R=4.1 \times 10^5$  °Csec/cm<sup>2</sup>, single-phase cells, two-phase cells, and three-phase composite structure. (a) Transverse section, 100X. (b) Longitudinal section, 100X.

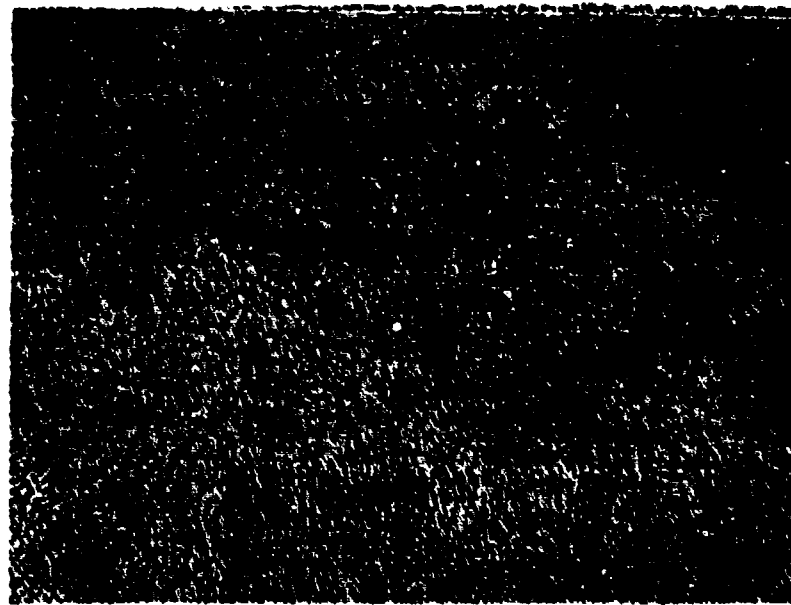


(a)

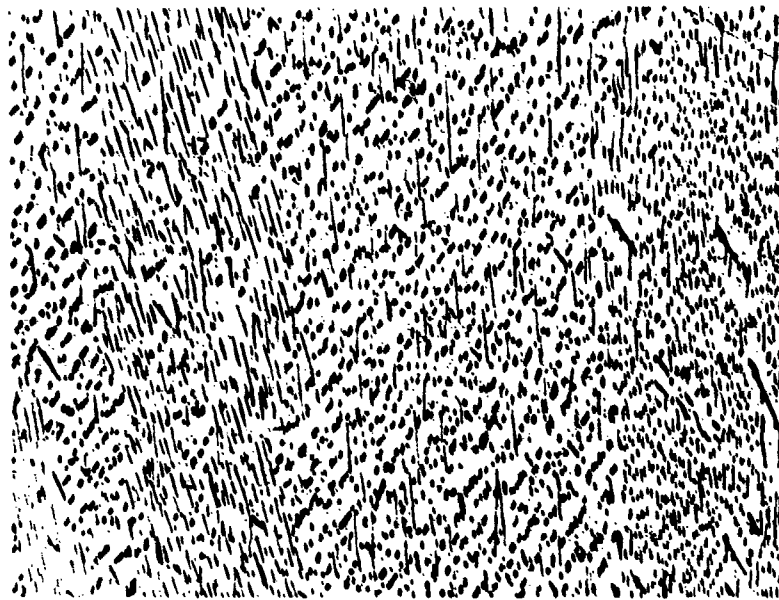


(b)

Figure 5. Ingot #26, 8.85 wt% Ni, 0.92 wt% Cu,  $G/R = 10.5 \times 10^5 \text{ } ^\circ\text{C sec/cm}^2$ , single-phase cells and two-phase composite. (a) Transverse section, 100X. (b) Longitudinal section, 100X.



(a)

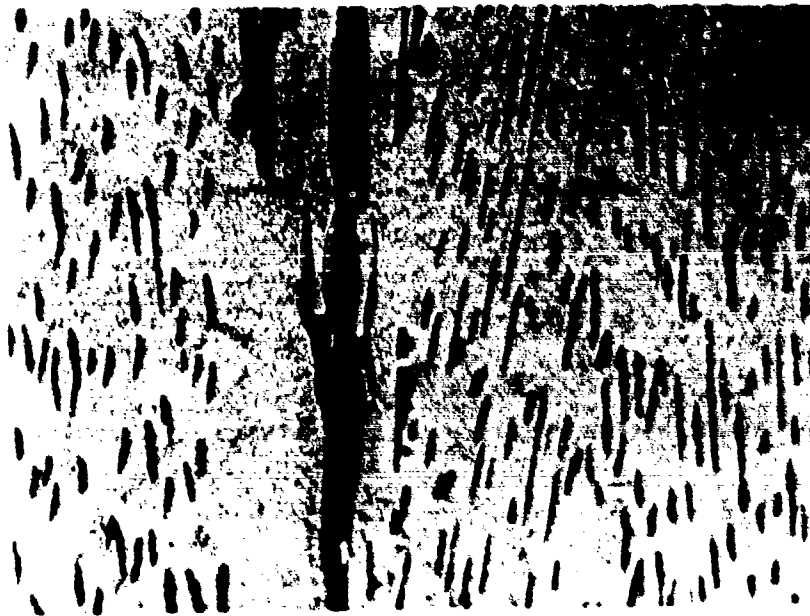


(b)

Figure 6. Ingot #11, 5.15 wt% Ni, 0.95 wt% Cu,  $G/R = 4.85 \times 10^5 \text{ }^\circ\text{Csec/cm}^2$ , two-phase composite structure. (a) Transverse section, 100X. (b) Longitudinal section, 100X.



(a)



(b)

Figure 7. (a) 1.5 wt% Cu + 5.85 wt% Ni,  $G/R=2.73 \times 10^5 \text{ } ^\circ\text{C sec/cm}^2$ , two-phase cells and three-phase composite structure. Transverse section, 200X (after Rinaldi Sharp and Flemings<sup>3</sup>). (b) Ingot #21, 6.6 wt% Ni + 1.01 wt% Cu,  $G/R = 1.94 \times 10^5 \text{ } ^\circ\text{Csec/cm}^2$ , single-phase cells, two-phase cells, and three-phase composite structure. Longitudinal section taken near the quenched liquid-solid interface, 500X.

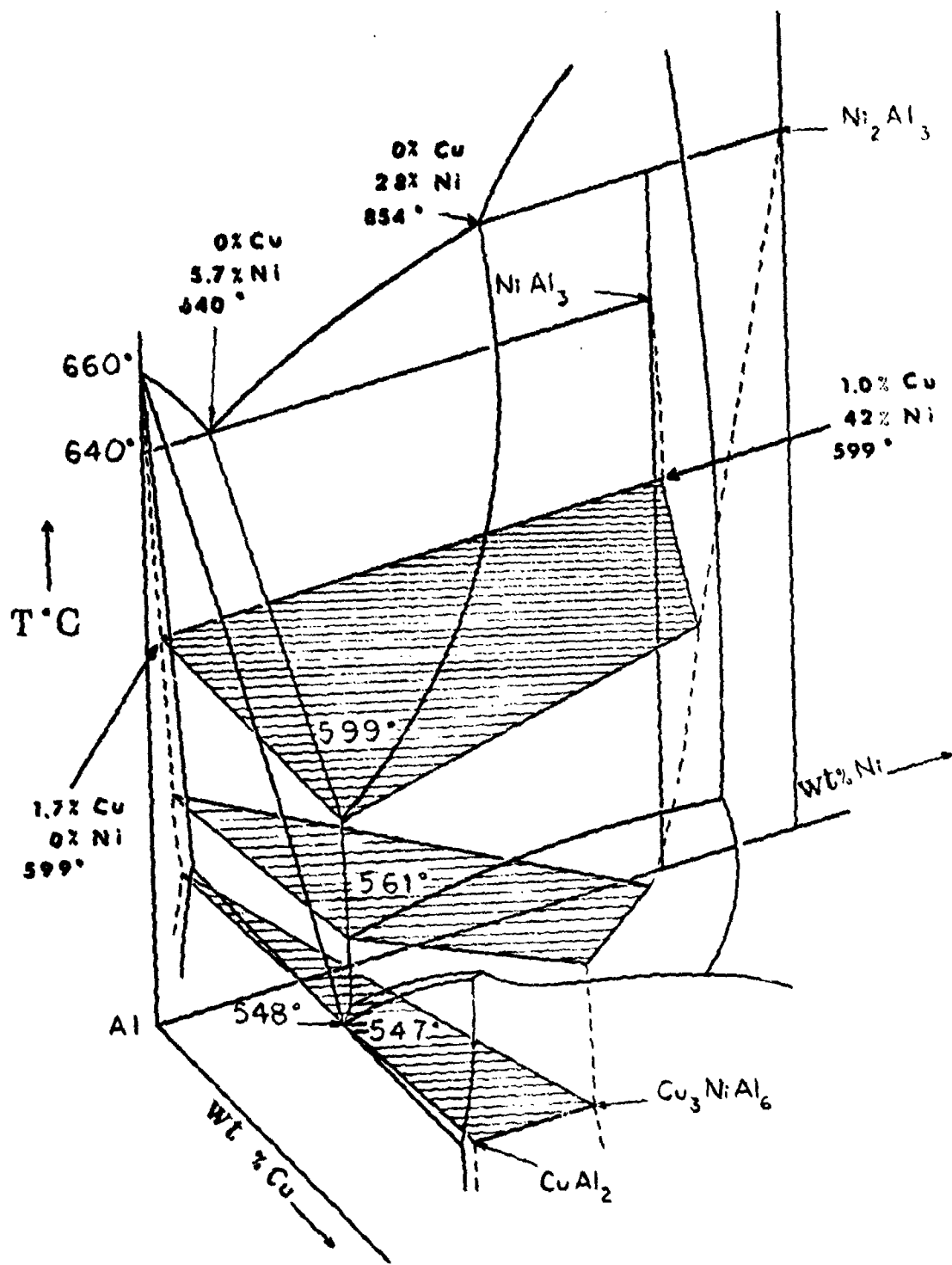


Figure 8. Aluminum-rich corner of Al-Cu-Ni system.

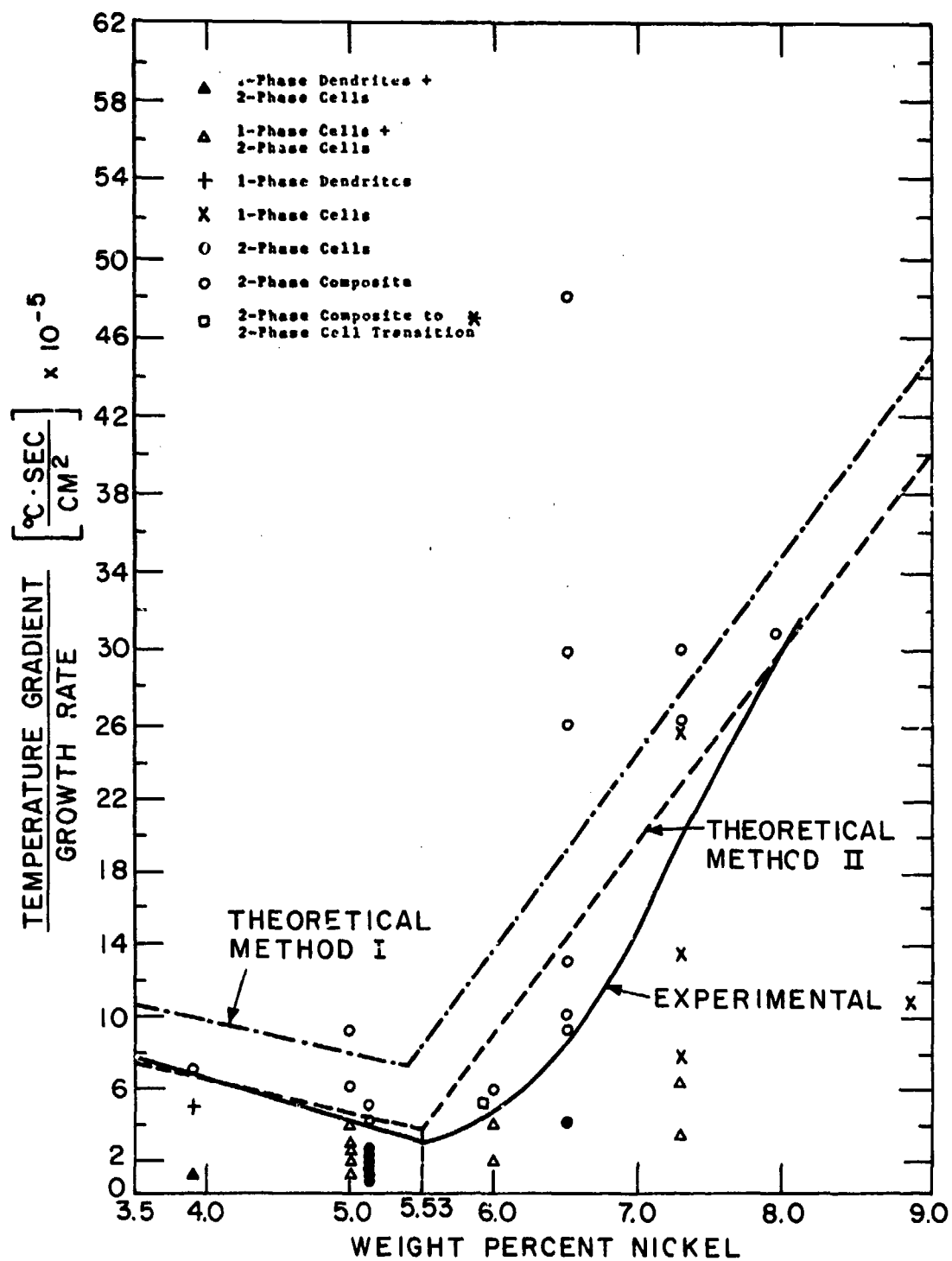


FIGURE 9. STRUCTURE OF DIRECTIONALLY SOLIDIFIED INGOTS AS A FUNCTION OF G/R AND  $C_{\text{Ni}}$  WITH  $C_{\text{Cu}} = 1 \text{ wt \% Cu}$ . \* REFERENCE RINALDI, SHARP AND FLEMINGS.

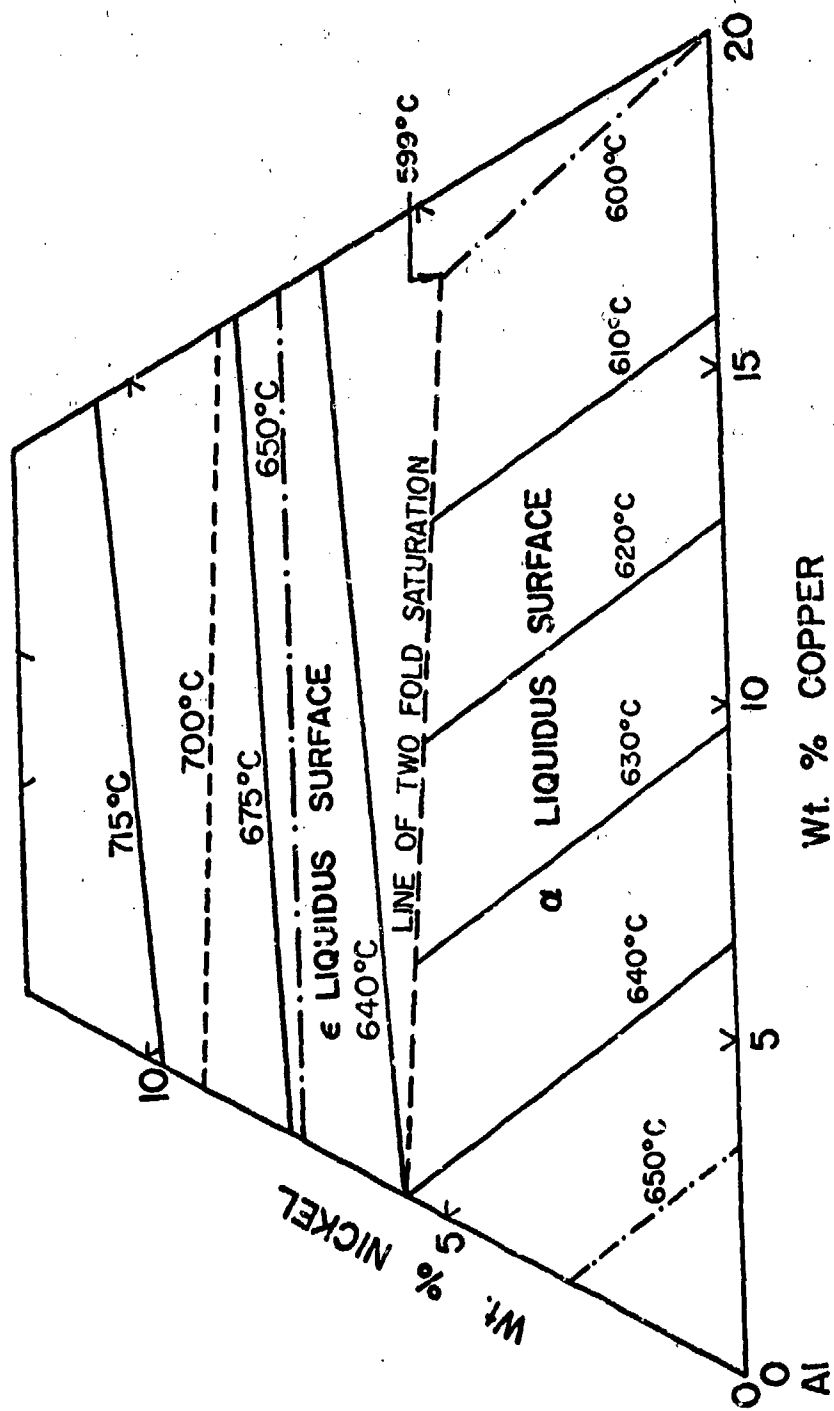


Figure 10. Al-Cu-Ni Liquidus Surface.

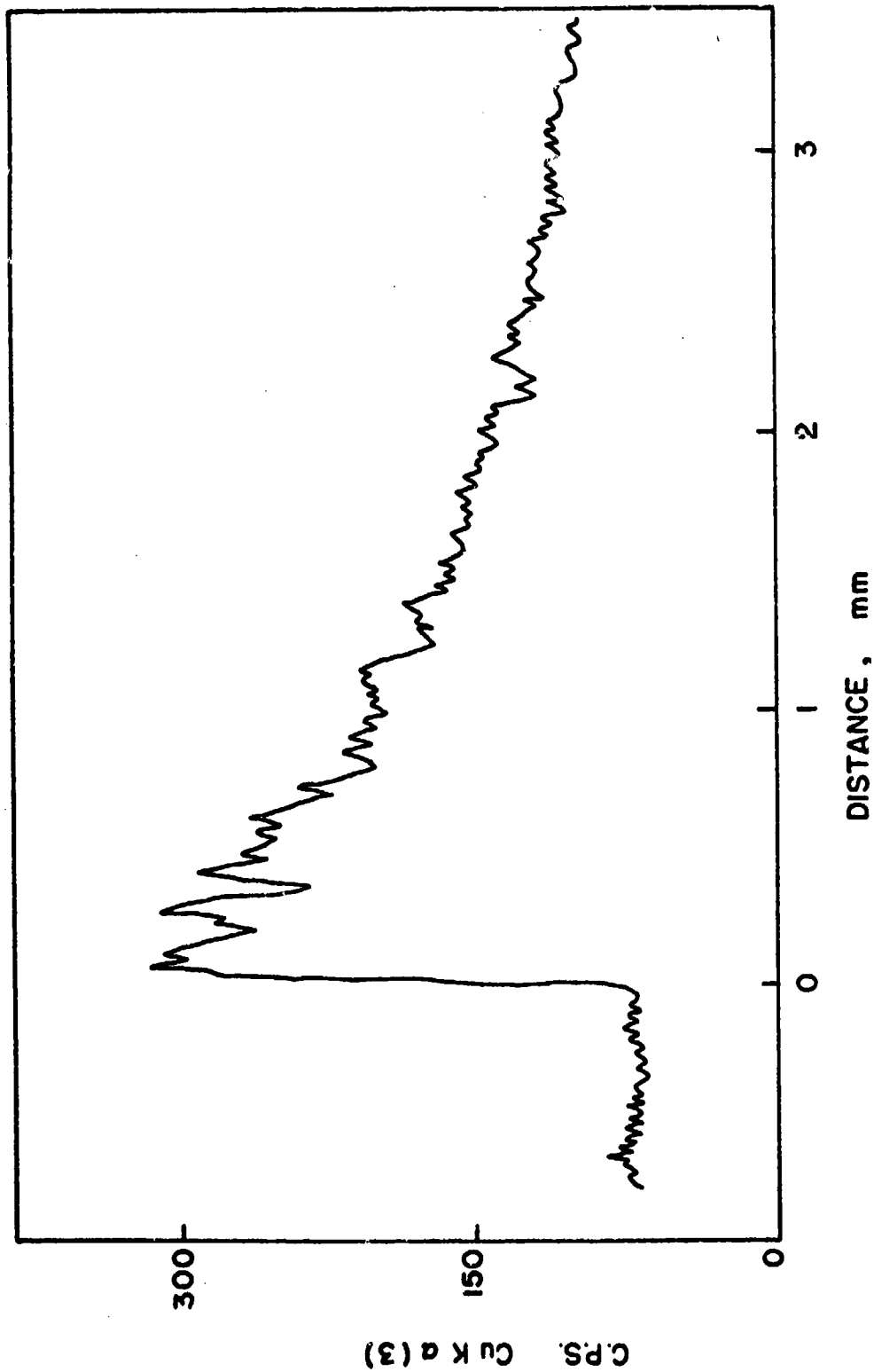


Figure 11. Cu distribution ahead of the quenched composite interface of ingot #1.

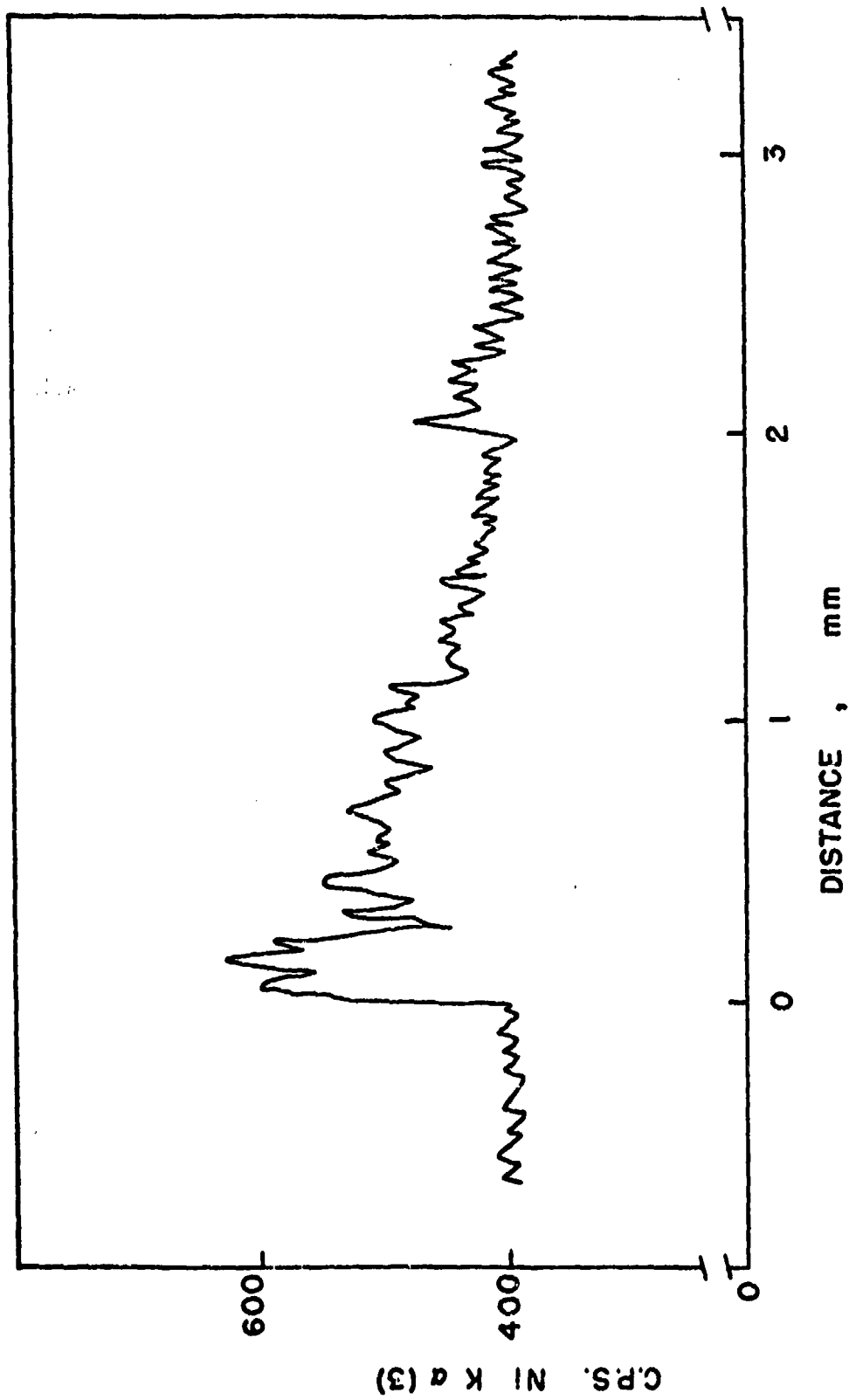


Figure 12. Ni distribution ahead of the quenched composite interface of ingot #1.

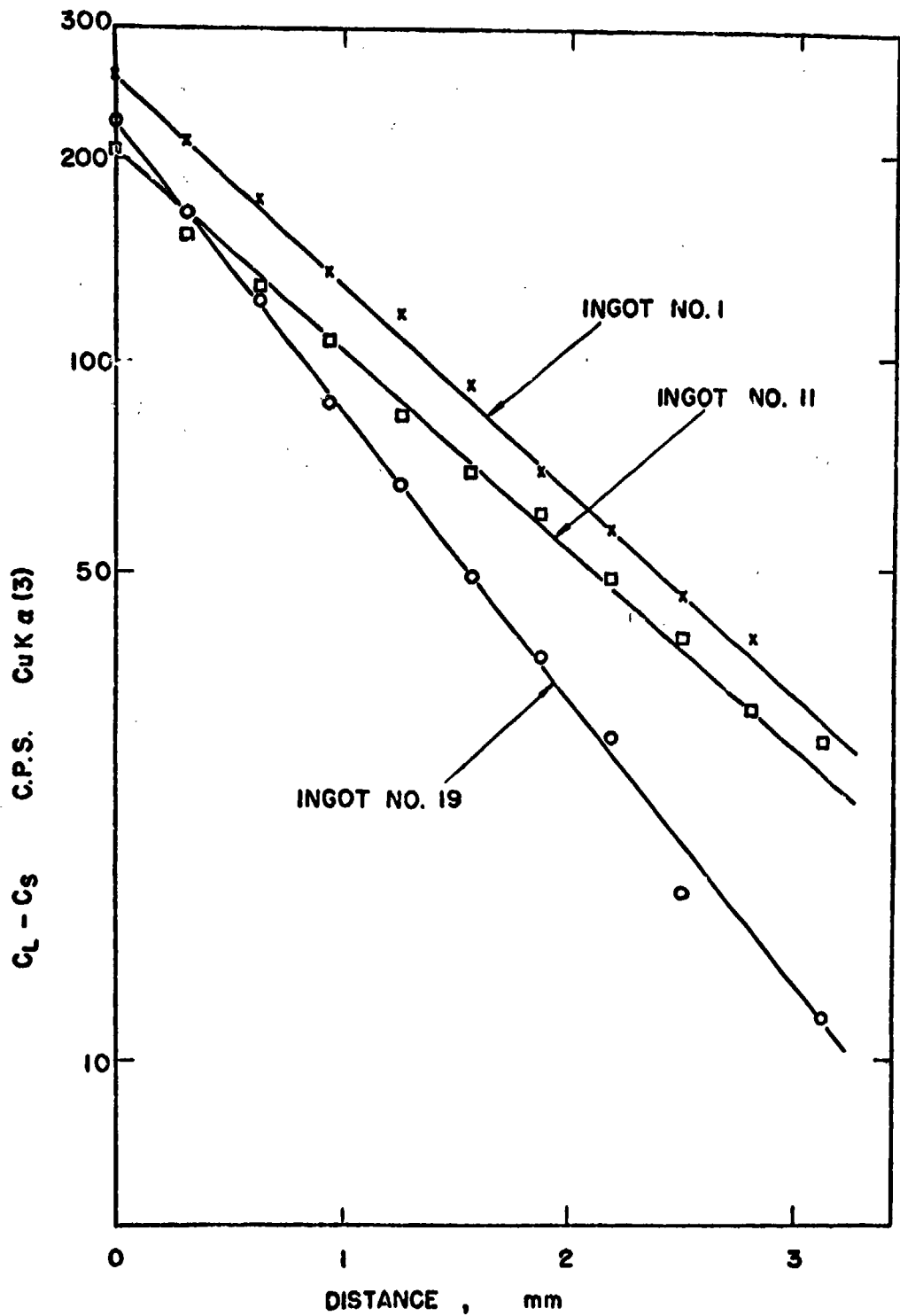


Figure 13.  $\ln(C_L - C_S)$  for Cu versus distance from the quenched interfaces in ingot #'s 1, 11 and 19.

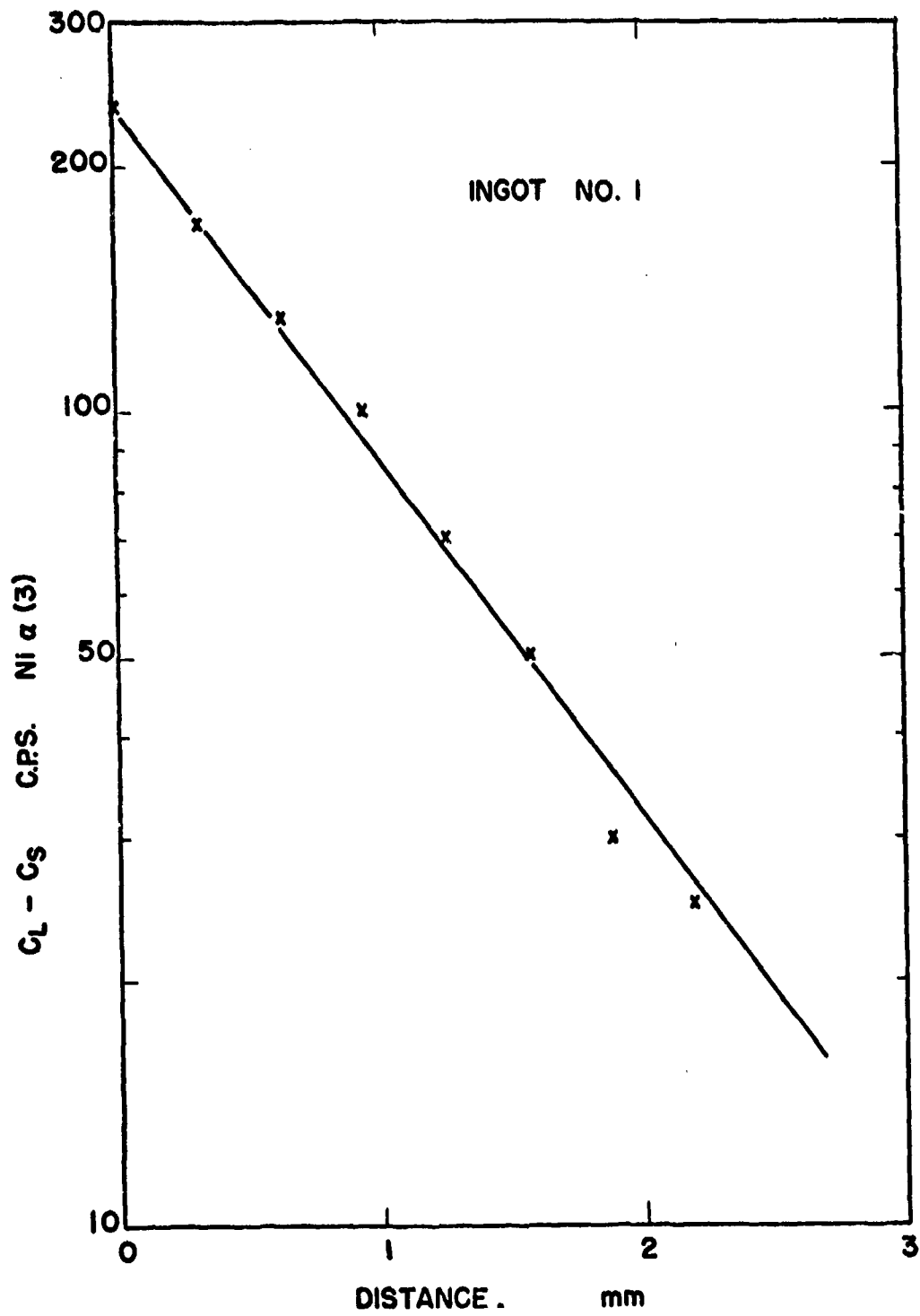


Figure 14.  $\ln(C_L - C_S)$  for Ni versus distance from the quenched interface in ingot #1.

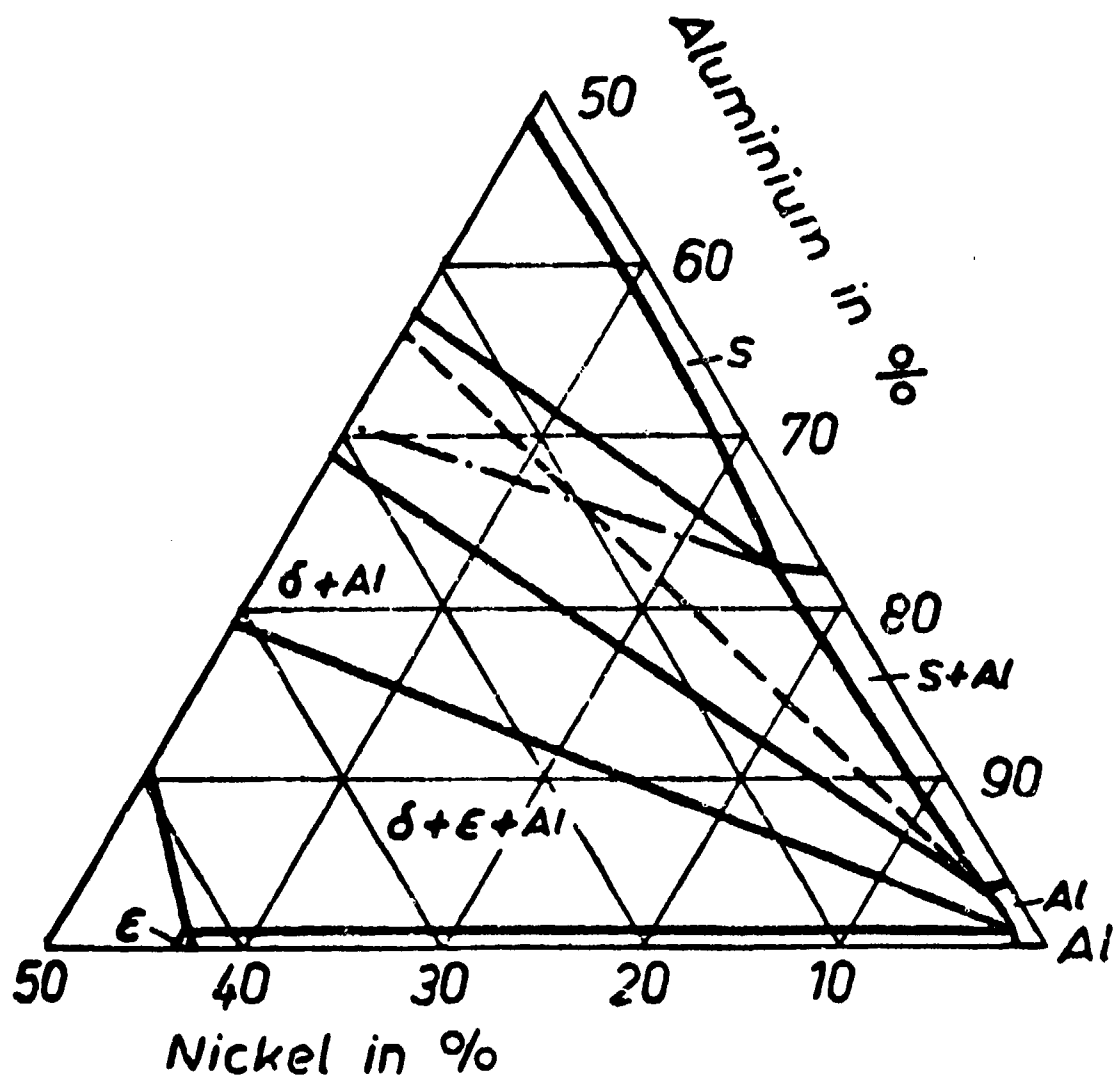


Figure 15. Al-Cu-Ni ternary system, 600°C isotherm (after Koster, Zwicker and Moeller<sup>14</sup>).

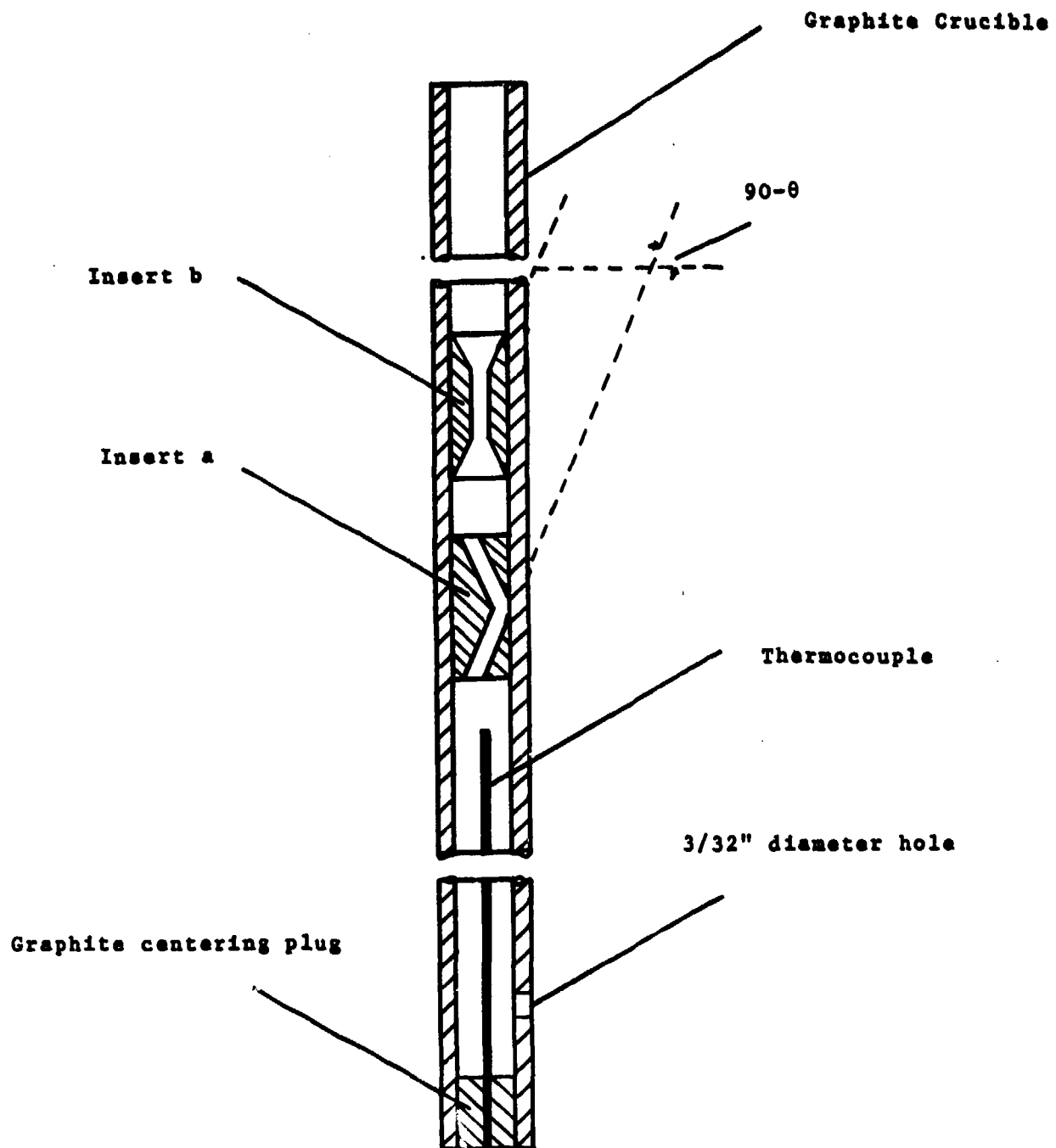
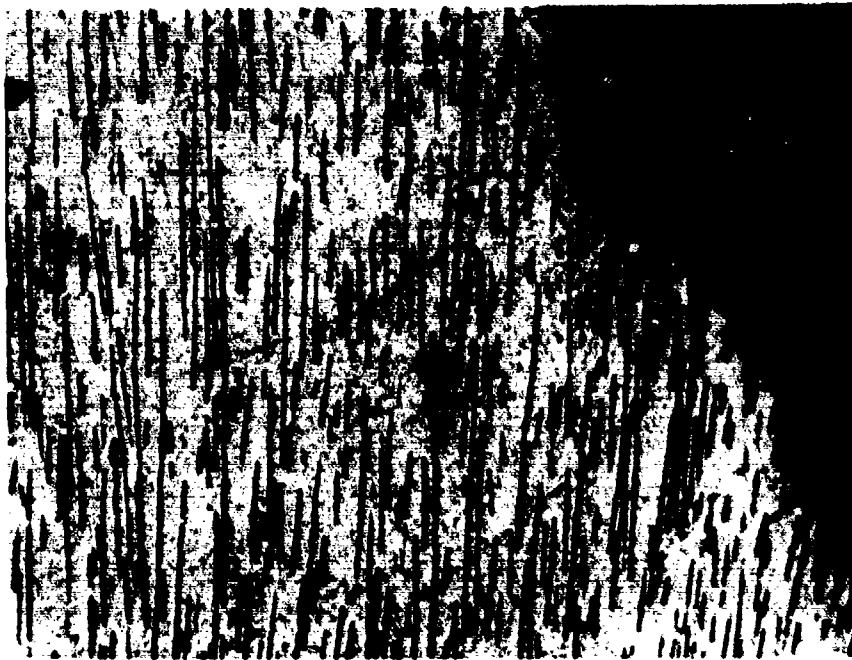
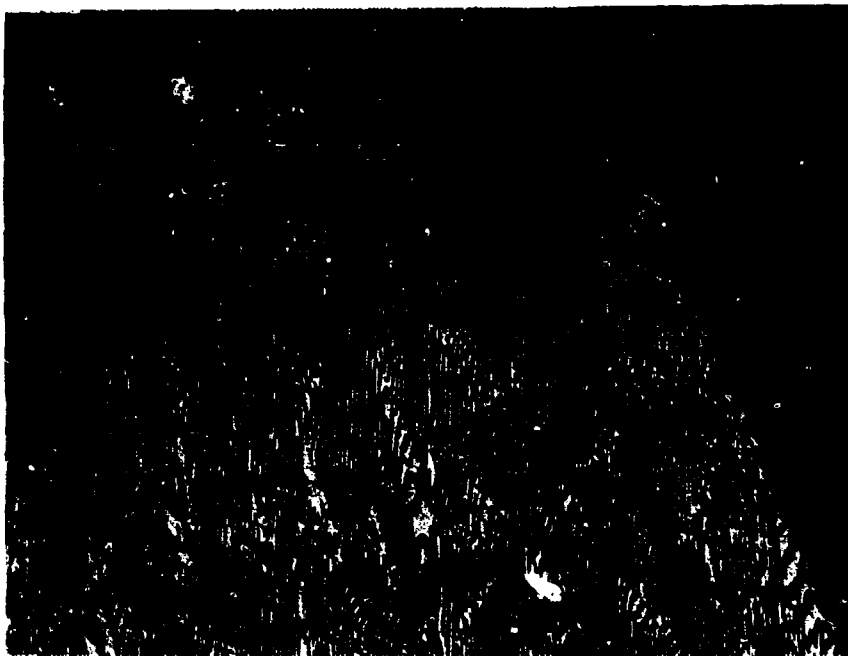


Figure 16. Cross-sectional view of crucible and insert system.



a.



b.

Figure 17. Insert b, lower portion, structure aligned in the original growth direction, longitudinal view, 115X. (a) Sample No. 0008, binary Al-Ni eutectic,  $\theta = 18^\circ$ . (b) Sample No. 0014, ternary Al-Ni-Cu eutectic,  $\theta = 10^\circ$ , corresponding schematic Figure 18.

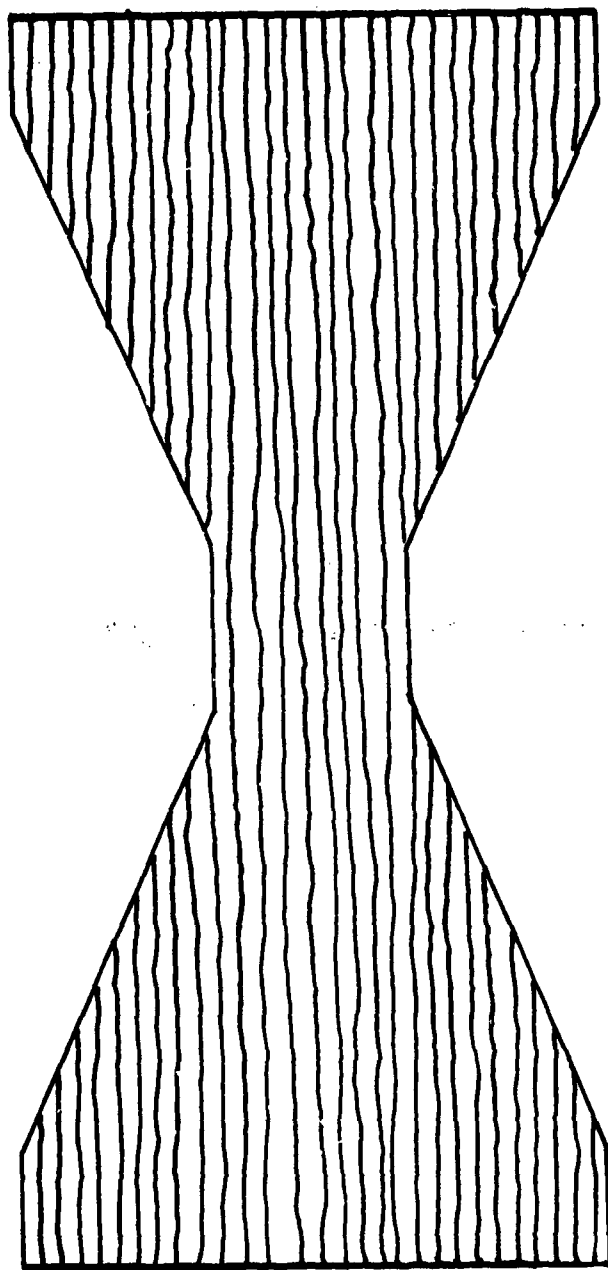
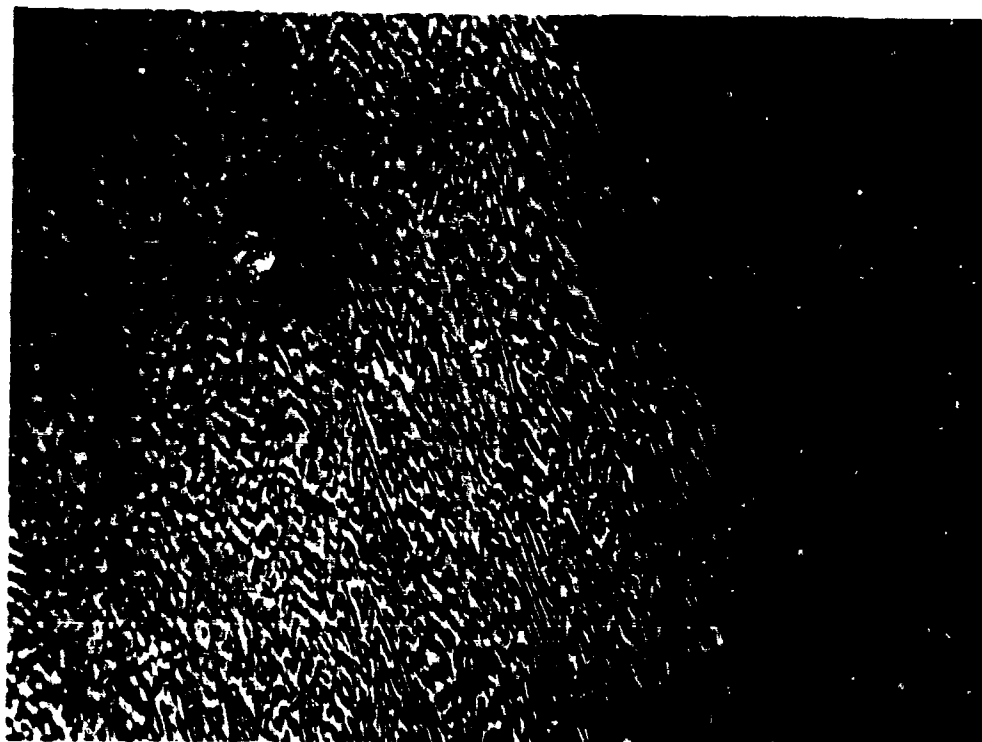


Figure 18. Schematic view of insert type b,  $\theta > 8^\circ$ , showing the structure orientated in the original growth direction.



**Figure 19.** Sample No. 0017, insert type b, ternary Al-Ni-Cu eutectic, upper portion, structure follow the contour of the insert,  $\theta = 6^\circ$ , longitudinal view, 115X. corresponding schematic Figure 20.

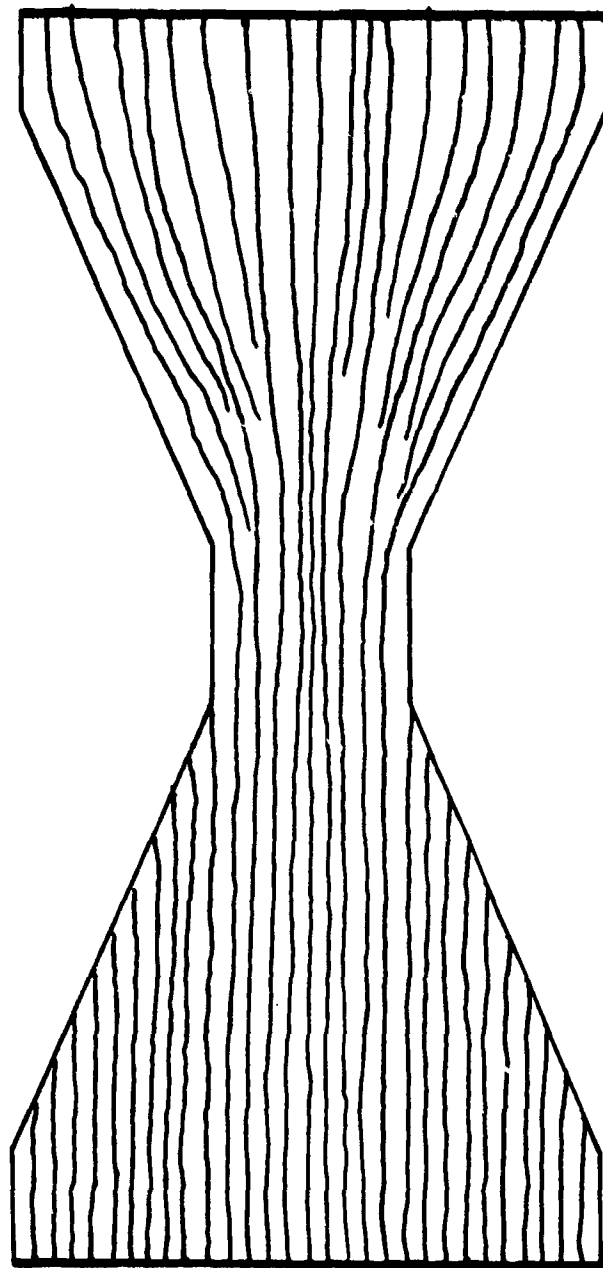


Figure 20. Schematic view of insert type b,  $\theta < 8^\circ$ , showing the structure following the contour of the insert at the upper portion.

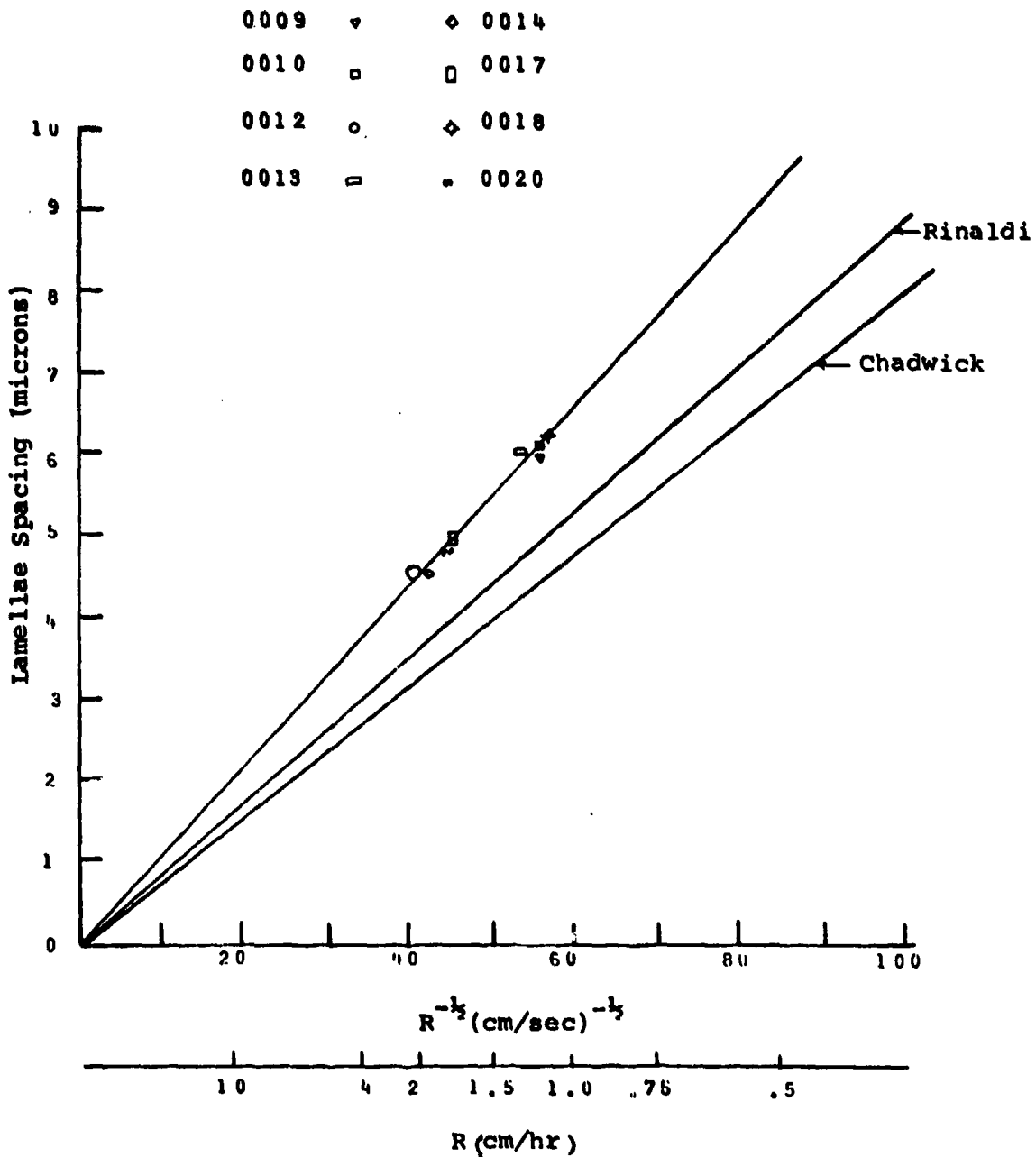


Figure 21. Lamellae spacing as a function of growth rate for ternary Al-Ni-Cu eutectic, Rinaldi's data<sup>3</sup> for compositions containing from 17.5 to 12.3 at. pct. Cu and from 0.0 to 1.32 at. pct. Ni, Chadwick's<sup>22</sup> data for the Al-Cu binary eutectic.

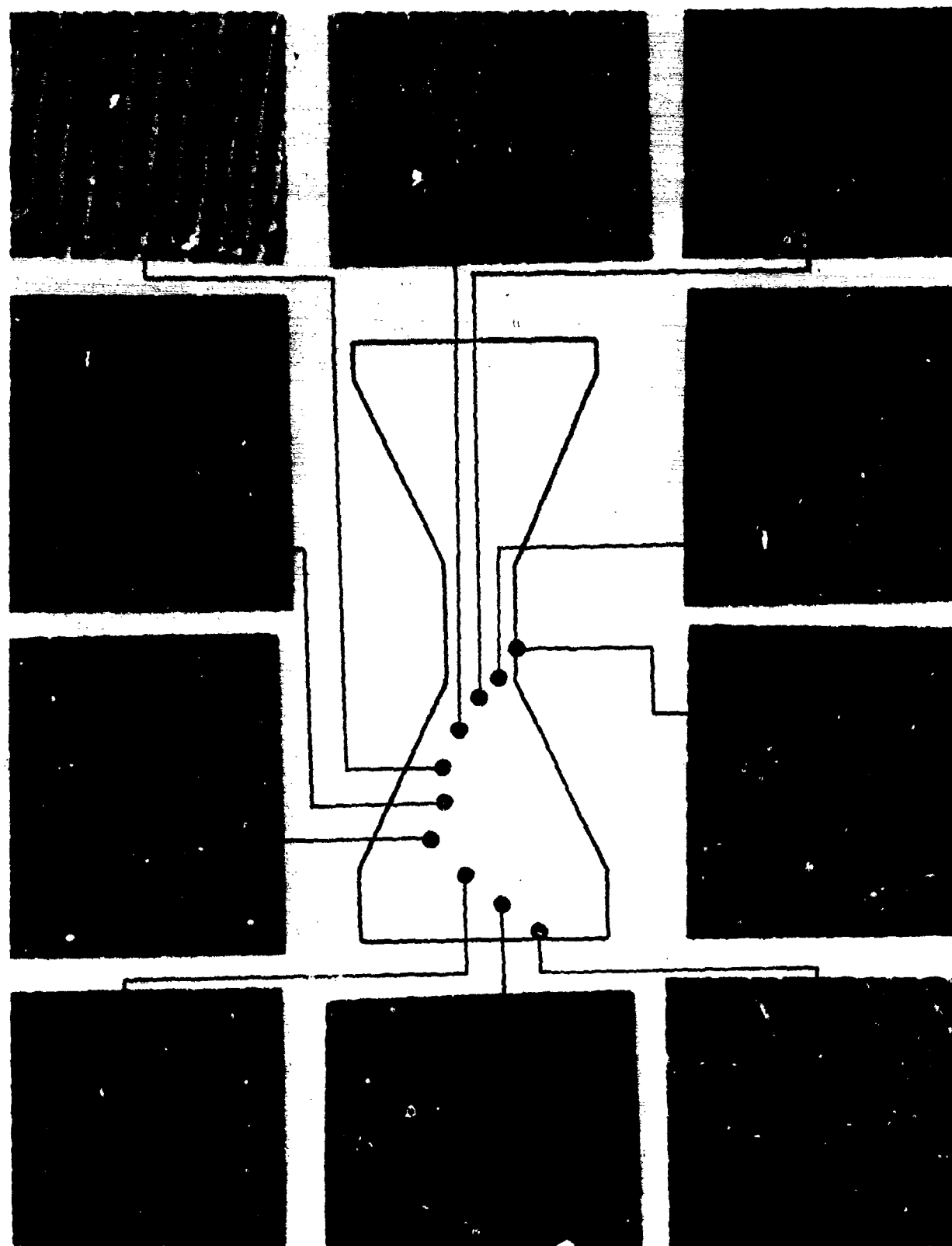


Figure 22. Sample No. 0014, ternary Al-Ni-Cu eutectic, transverse view, 1150X.

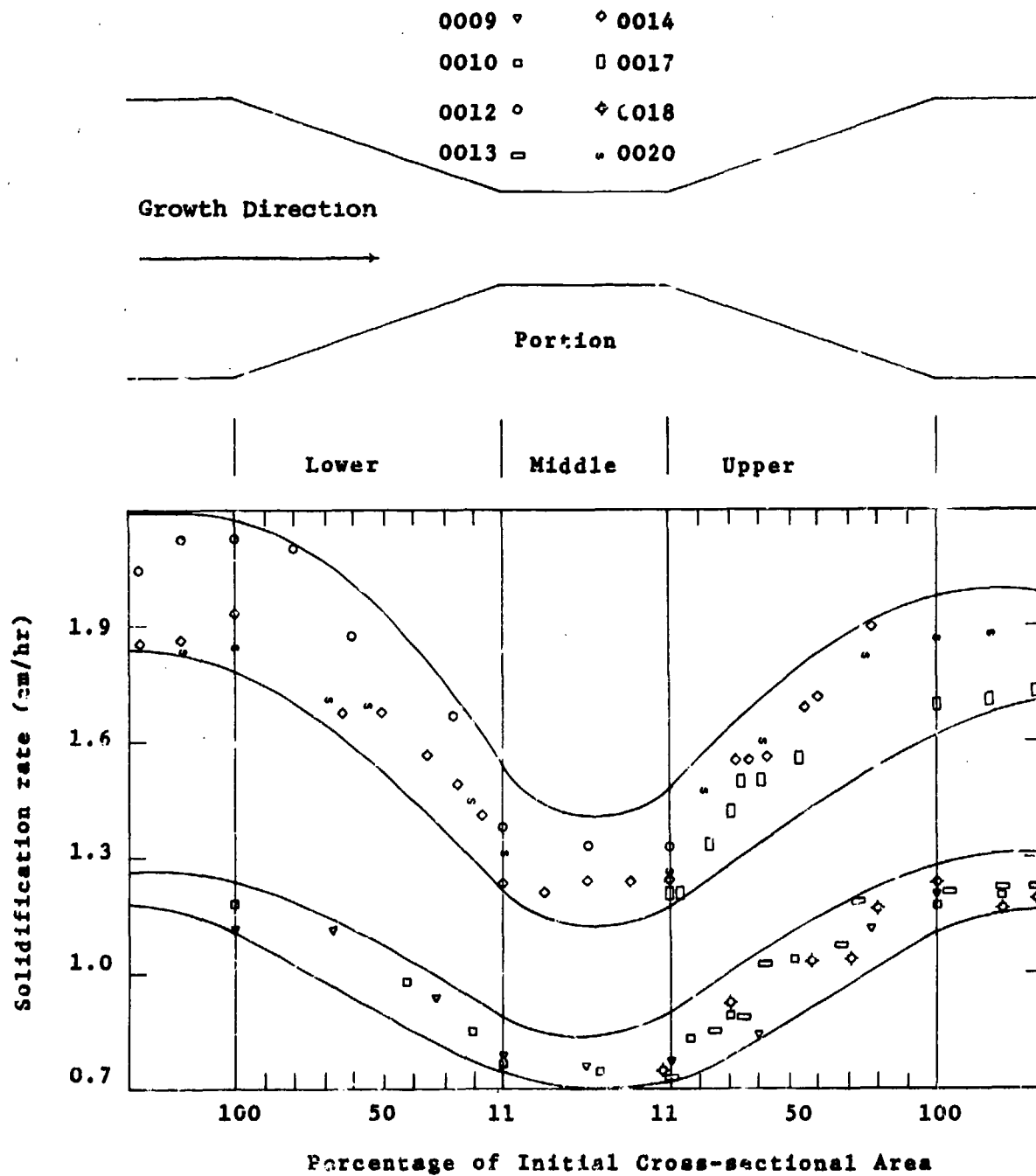


Figure 23. Solidification rate at various percentages of initial cross-sectional area into the portions of insert type b, ternary Al-Ni-Cu eutectic.

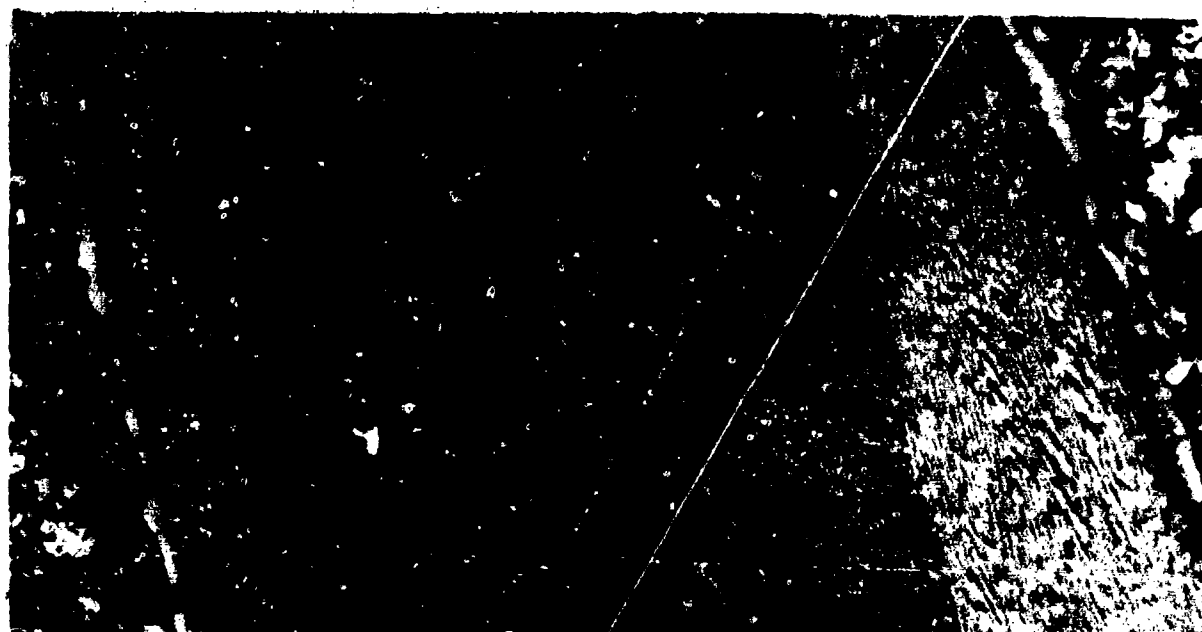
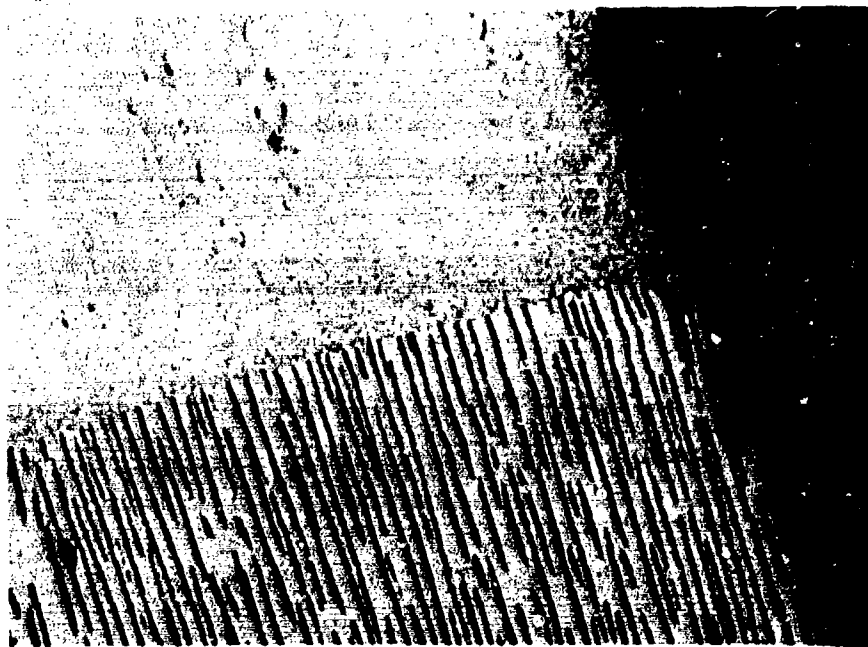


Figure 24. Sample No. 0020, insert type a, ternary Al-Ni-Cu eutectic, lower portion, viewed under polarized light,  $\theta = 20^\circ$ , longitudinal view, 115X.



a.

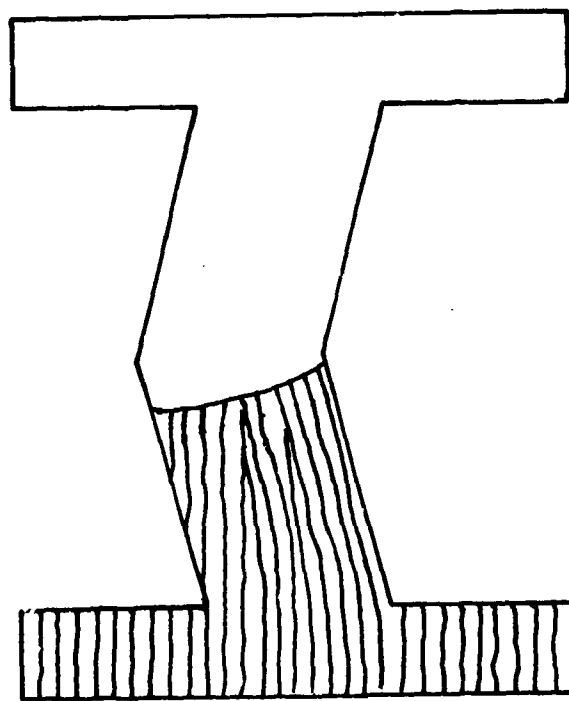
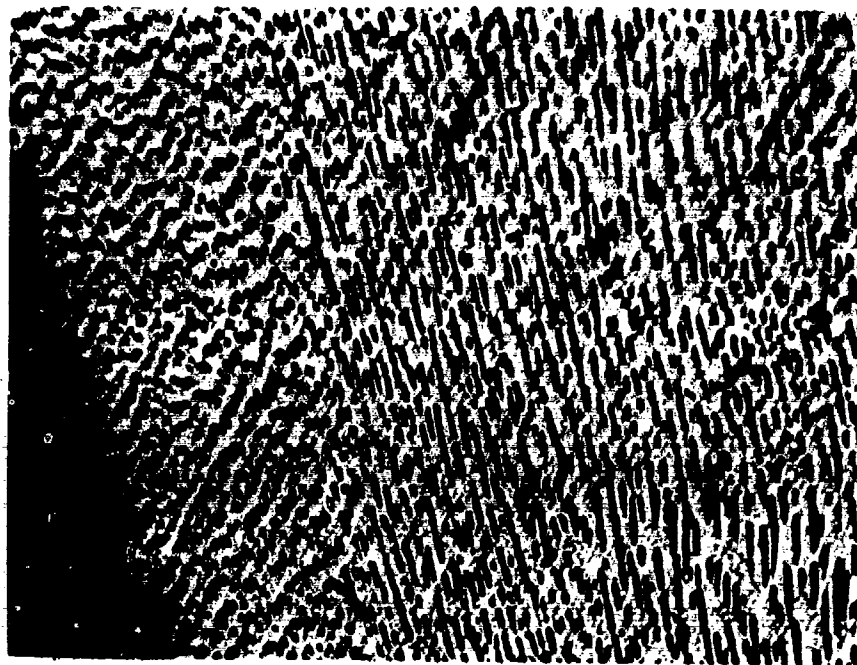
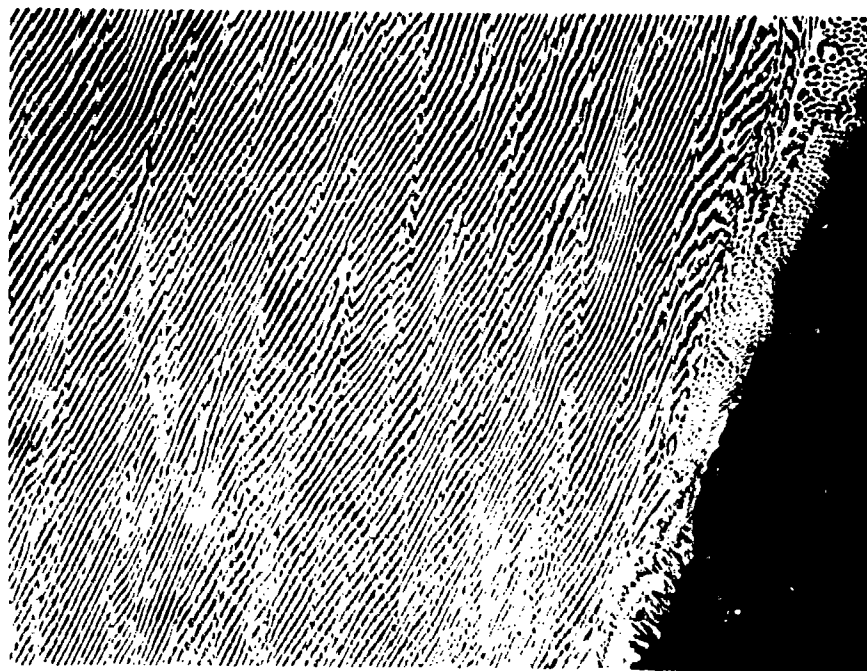


Figure 25. (a) Sample No. 0003, insert type a, binary Al-Ni eutectic, lower portion, location of liquid-solid interface,  $\theta = 14^\circ$ , longitudinal view, 115X. (b) Schematic.



a.



b.

Figure 26. Insert type a, middle portion after the bend, downward face, depleted zone, longitudinal view, 115X. (a) Sample No. 0004, binary Al-Ni,  $\theta = 14^\circ$ . (b) Sample No. 0013, ternary Al-Ni-Cu,  $\theta = 14^\circ$ , corresponding schematic Figure 27.

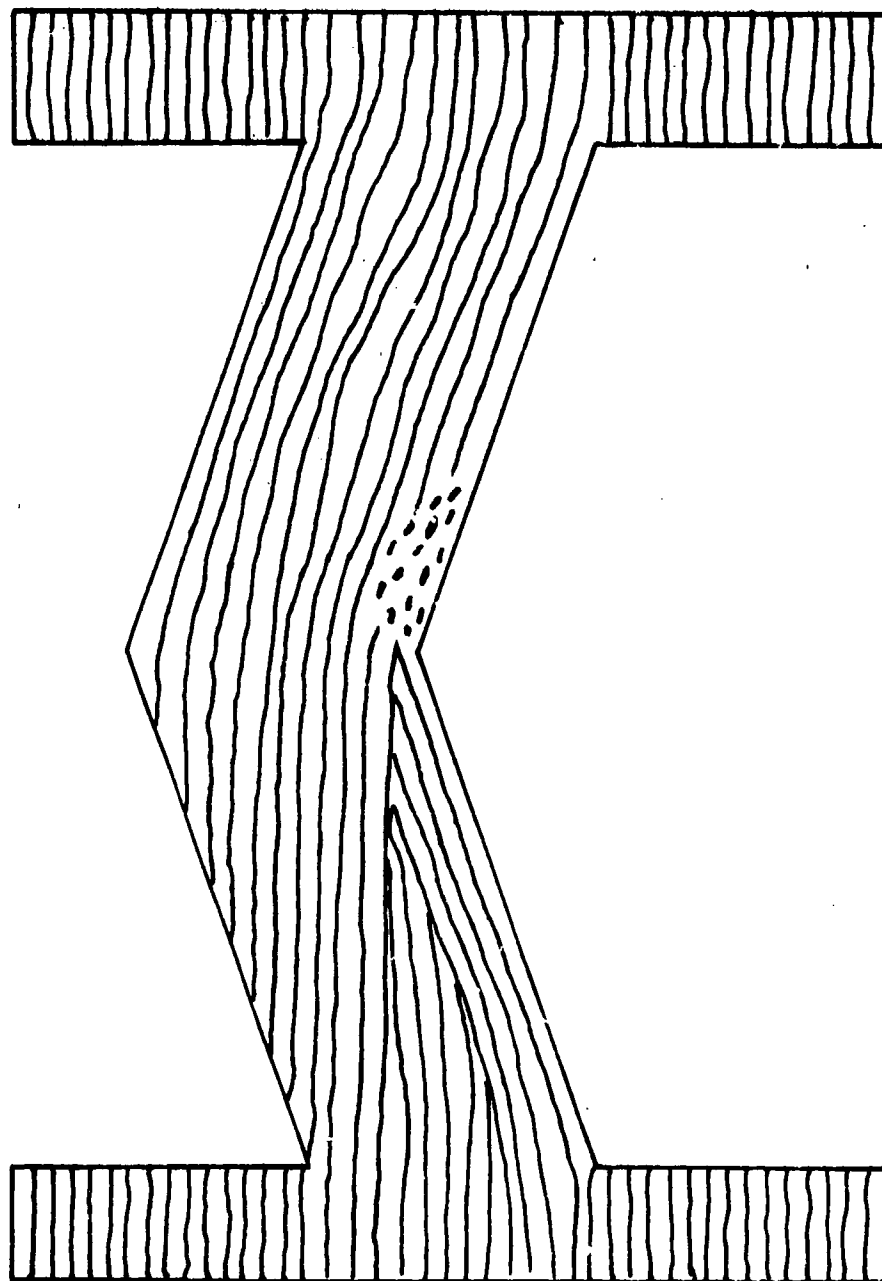


Figure 27. Schematic view of insert type a,  $\theta > 8^\circ$ , showing the different grain orientations developed.

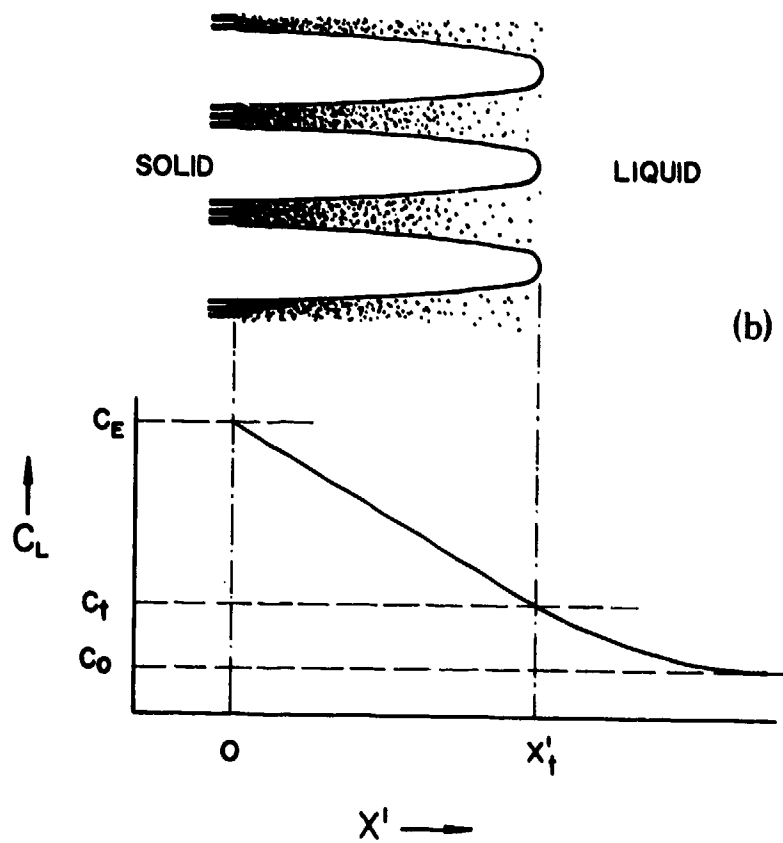
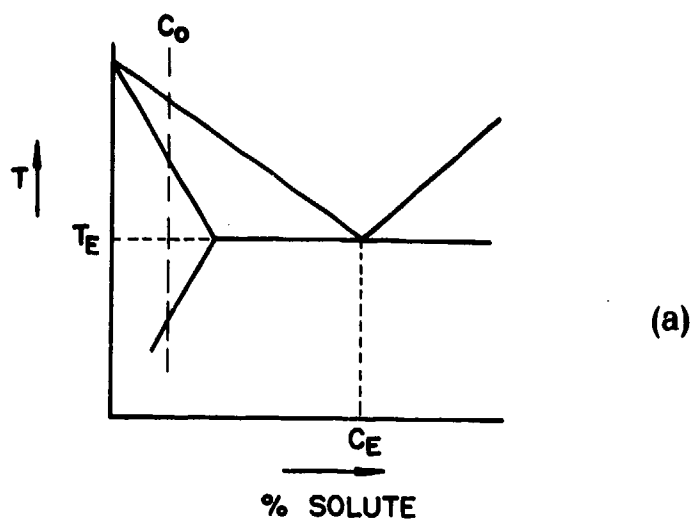


Figure 28. Schematic illustration of the unidirectional solidification of cells of a binary alloy: (a) phase diagram, (b) showing the concentration of solute as a function of distance.

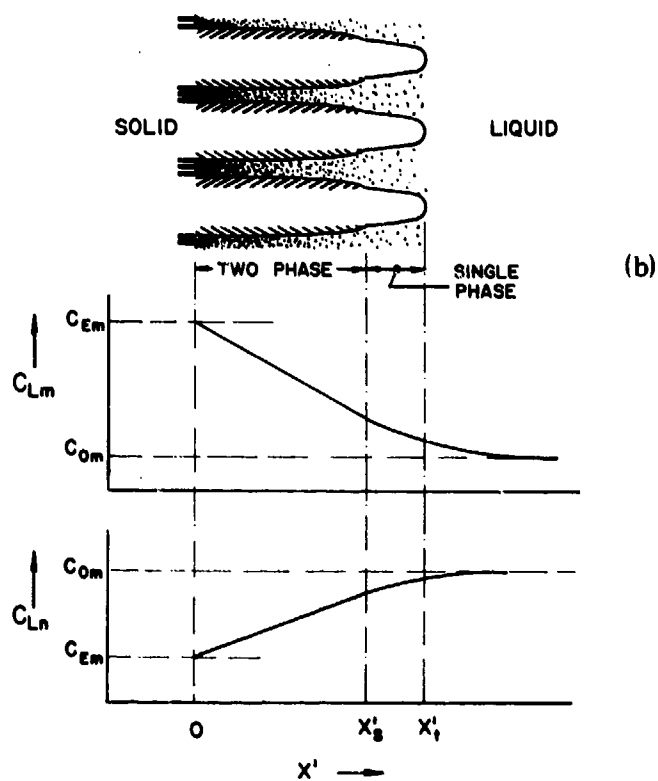
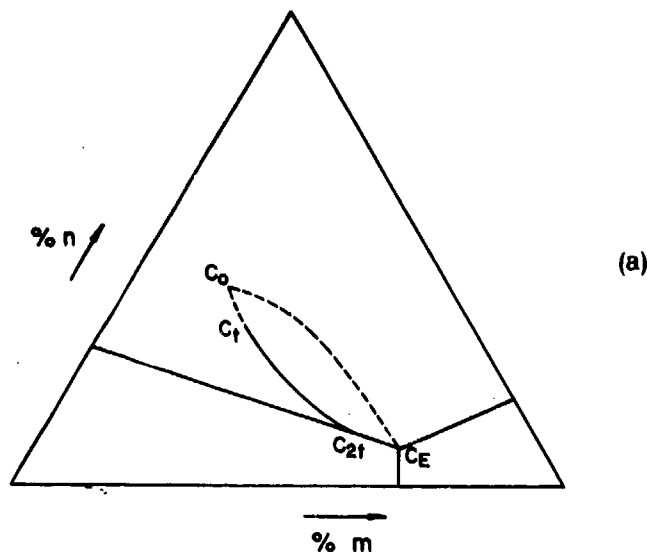


Figure 29. Schematic illustration showing the growth of cells or dendrites in a ternary system. (a) Phase diagram showing solidification path (full line) and diffusion path for a planar interface (dashed line). (b) Intercellular liquid composition. Primary phase solidifies first and, when the liquid composition reaches  $C_{2t}$ , two-phase material is formed.

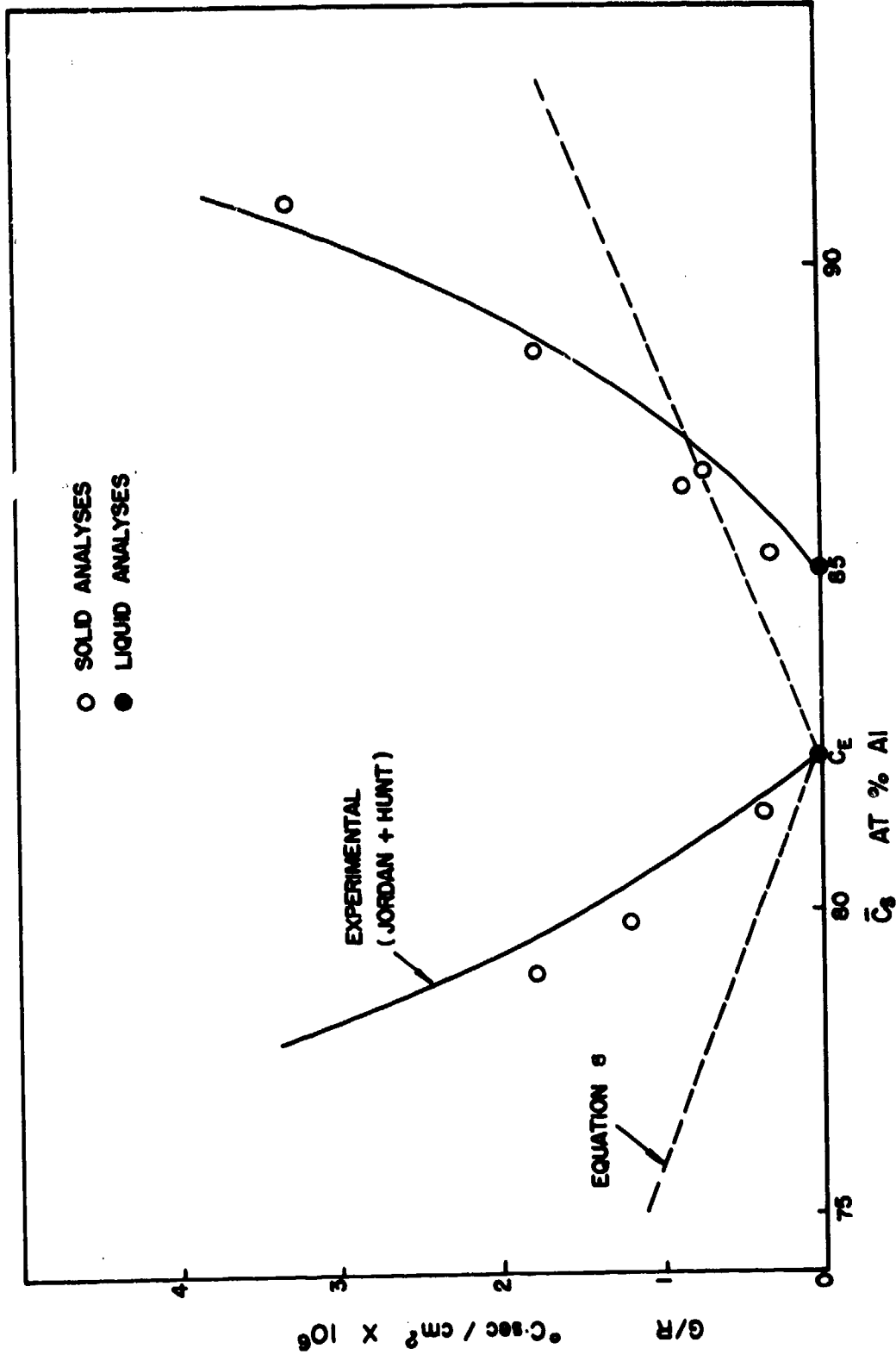


Figure 30. Average concentration of interdendritic eutectic plotted as a function of  $G/R$  for the binary Al-CuAl<sub>2</sub> system. Also included are the theoretical lines calculated from equation 8 and the experimental results of Jordan and Hunt.<sup>24</sup>

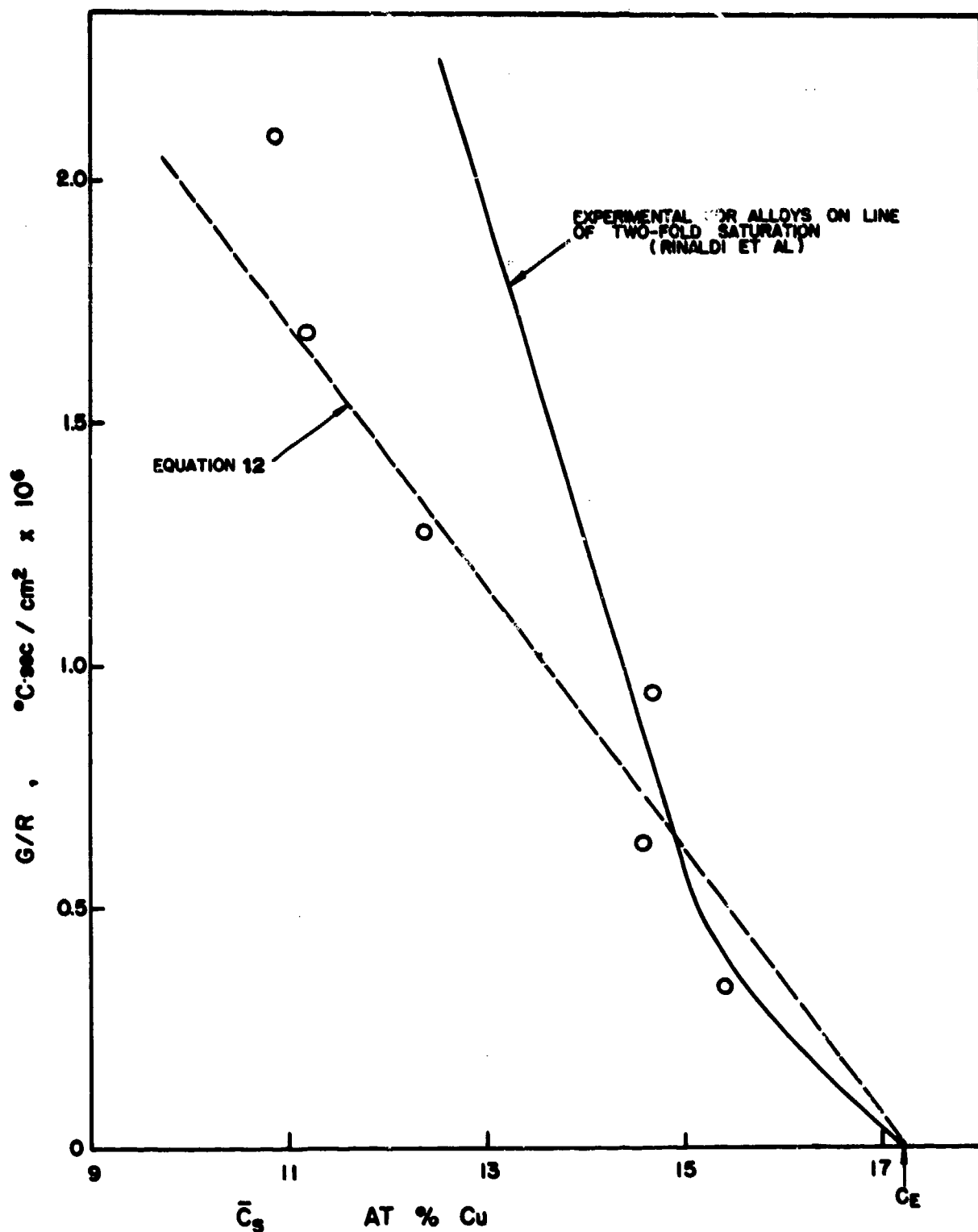


Figure 31. Average copper concentrations of interdendritic eutectic plotted as in Figure 3 for ternary Al-Cu-Ni system. The theoretical line is calculated from equation 12.